2008-04-09

AC-Calorimetry and Dielectric Spectroscopy on Anisotropic Liquid Crystal and Aerosil Dispersions

Florentin I. Cruceanu
Worcester Polytechnic Institute

AC-CALORIMETRY AND DIELECTRIC SPECTROSCOPY ON ANISOTROPIC LIQUID CRYSTAL AND AEROSIL DISPERSIONS

by

Florentin I. Cruceanu

A Dissertation
Submitted to the Faculty
of the

WORCESTER POLYTECHNIC INSTITUTE

In partial fulfillment of the requirements for the
Degree of Doctor of Philosophy
in
Physics
by

November 27, 2007

APPROVED:

Germano S. Iannacchione, Associate Professor and Head of Physics, WPI, Advisor

---

Rafael Garcia, Assistant Professor, Dept. of Physics, WPI

Ilie Fishtik, Research Associate Professor, Dept. of Chemical Engineering, WPI

Abstract

This thesis presents an experimental study of the influence of an external field and alignment upon a colloid of a liquid crystal (octylcyanobiphenyl denoted 8CB) and a silica gel of aerosil nano-particles. The first techniques used was an AC-calorimetry (alternating current heating) and the systems under investigation were firstly put under the influence of a magnetic field at John Hopkins University in Baltimore by professor Leheny's group. The experiments revealed changes in transition temperatures, nematic range and critical coefficient that could account for what we called a "memory" of the above mentioned structures.

The second technique, dielectric spectroscopy, was applied to the same very densities of mixtures mentioned in the first paragraph. The samples were applied in one procedure an increasingly higher alternating electric field. An overall increase of the capacitance of the sample was measured. The second experiment was to reproduce the application of the magnetic field from the AC-calorimetry experiment now with an electric field. In dielectric spectroscopy case, an increase in transition temperature after the application of the procedure was revealed.

Table of Contents

List of Figures

List of Tables

List of Symbols

A	area, Landau free energy phenomenological parameter
$A^{\pm}$	heat capacity critical amplitudes
α	heat capacity critical exponent
$B^{\pm}$	heat capacity critical backgrounds
B	Landau free energy phenomenological parameter
β	order parameter critical exponent
C	heat capacity, Landau free energy phenomenological parameter
C_p	specific heat capacity
ΔC_p	excess specific heat capacity
ΔC_B	excess effective specific heat capacity, $\Delta C_B = C_p^{(NAS)} - C_p^{(AC)}(coex)$
$C\,'$	real heat capacity
$C\,''$	imaginary heat capacity
C^*	preliminary measured heat capacity
γ	susceptibility critical exponent
D	Landau free energy phenomenological parameter
$D^{\pm}$	correction to scaling amplitudes
d	dimensionality of a system, sample thickness
Δ	correction to scaling exponent
δ	equation of state critical exponent

E	energy
F	Landau free energy
f	Landau free energy density
$G^{(2)}$	intensity-intensity autocorrelation function
H	enthalpy, magnetic field intensity
δH	transition enthalpy
δH^*	effective transition enthalpy as measured from AC calorimetry
$\delta H''$	imaginary transition enthalpy
ΔH	latent heat
h	random field interaction strength
I	light intensity, current intensity
i	imaginary constant $= \sqrt{-1}$
η	pair correlation length critical exponent
J	spin-spin exchange interaction
$\vec{k}$	wavevector,
k, k_0	wavevector amplitude, $k_0 = 2\pi/\lambda$
L	coupling constant of the Landau free energy
ℓ_θ	thermal diffusion length
λ	wavelength
M	magnetization
m	magnetization density
n	refractive index
Δn	birefringence
$\hat{n}$	nematic director
ν	correlation length critical exponent
ω	frequency of AC power, tilt angle of SmC phase

Ω	solid angle
P	pressure
P_0	amplitude of AC power
Ψ	*N-A* complex order parameter
Q	heat
Q_{ij}	*I-N* tensor order parameter
$\vec{q}$	scattering wave vector
q	scattering wave vector amplitude
R	thermal resistance, radius, ohmic resistance
$\vec{r}$	position vector
r	position vector amplitude
ρ	density
ρ_S	conjugate density, (grams of silica per volume of liquid crystal)
ϱ	*Sma-SmC* order parameter
S	entropy, *I-N* scalar order parameter
σ	diffusion crosssection
T	temperature
T_{AC}	amplitude of temperature oscillations
t	reduced temperature, time
τ	characteristic time constant, turbidity
T_c	critical temperature
T^{**}	nematic superheating temperature
U	internal Energy
V	volume
ξ_N	nematic correlation length
W	work

Φ	absolute phase shift between temperature and power oscillations
ϕ, θ, ω	angles
ϕ_N	nematic fraction
φ	relative phase shift between temperature and power oscillations, phase of *Sma-SmC* order parameter

Acknowledgments

I could not pursue this endeavor without the help of Professor Germano Silvio Iannacchione. He pushed me into it and every thing I wrote is also his achievement. Part of this Thesis is a collaboration with Professor Leheny's group at John Hopkins University in Baltimore. I deeply thank them for this opportunity.

I would like to thank Professor Rafael Garcia and Professor Ilie Fishtik for the very good feedback they gave me with this thesis as well as serving on my thesis committee.

I would like to thank Jacqueline Malone and Roger Steele for all their help.

I would like to thank everyone who help me in any possible way to finish the present document

This work is dedicated to my faithful and loving wife, my two wonderful daughters, and to my parents.

Chapter 1

INTRODUCTION

1.1 Introduction

A very important topic these days in Physics is the so called "complex fluids". One of the systems in this category is a liquid that is mixed with a solid component that arranges itself in a steady or at least quasi-steady structure. These structures have drawn the attention of an increasing number of physicists lately. Not only the industrial world, which is interested in additives that can improve the quality of a paint for example, but also in biology this might have an interesting future if one only considers the cholesterol in blood vessels. In order to understand the basics, it is necessary to use a system such as the well-known 8CB liquid crystal mixed with silica beads. The novelty in this thesis is the study of the influence of the magnetic and electric fields against the system just mentioned.

In this work, we try to explain the permanent changes of the mixture due to the process. An earlier attempt was performed by the means of X-rays scattering Ref. [16] and [48]. The first technique used here is AC-calorimetry. In order to analyze the results, we present different parameters of the phase transitions before and after the process we call alignment. In most cases we found differences that prove the influence of the magnetic field. The second technique, dielectric spectroscopy, was used to reveal the influence of a electric field against the same concentrations of the mixtures mentioned above.

1.2 Liquid Crystals

The first part of the colloidal mixture and the main object of our study is the liquid crystal, a transitory system between liquids and crystals, displaying properties from both constituents of its name but also new and unique ones. There exists a wide variety of liquid crystals based on the geometry of constitutive elements and the way these come together. There are two main reasons for the formation of the liquid crystal phase, as follows. The first is the basic geometrical form of the molecules - mostly rods and disks - which allows close, quasiparallel packing in what is known as a monophillic liquid crystal. The second is an intramolecular interaction which causes micro-phase-separation of different parts of the molecule (an amphyphyllic liquid crystal).

Typical chemical substances that have liquid crystal phases are: cholesterol, esters, surfactants, glycolipids, phenyl benzoates, cellulose derivatives, paraffins, etc. Historically, the first liquid crystal discovered was cholesterol. The very cholesterol that is linked to stokes and heart attacks. In discussing applications, by far the most important is the liquid crystal display, but one must not overlook solvents for NMR used in temperature measurements, dyes, membranes and some others.

Under the name of liquid crystal there are actually more than one phase. The most common of them is nematic. In terms of resemblance, this is the closest to the liquid state which is also named isotropic from the property of the density function to have the same value in any direction. Actually, this density of particles function and the "density-density correlation function" represent the tools that will show the characteristics of the liquid crystal. The latter has the mathematical representation:

$$< \rho(x)\rho(x^{'}) > \tag{1.1}$$

and for a liquid crystal this is a periodical function of a basic vector $\overrightarrow{x} - \overrightarrow{x^{'}}$. Hence, if there is no positional order or, in other words no correlation, we have an isotropic state. If the correlation function is not isotropic and the molecules are, on average, pointing in one direction, the state it is called nematic. If the substance start forming layers, the state is smectic. It is very important to mention that still exists diffusion of the molecules between the layers in smectic, or a tumbling mode

in nematic. Thus, the director in nematic and the layers in smectic are only in a statistical way.

The most important parameter in the study of liquid crystals is the order parameter. Choosing a parameter that should reflect the order is not that easy due to the requirement of relevance throughout all the possible processes the liquid crystal may encounter. The simplest nonzero parameter to be chosen is:

$$S = \frac{1}{2} < (3\cos^2\theta - 1) >= \int f(\theta)\frac{1}{2}(3\cos^2\theta - 1)d\Omega \tag{1.2}$$

this is the second term in the multipole expansion, the first one being null due to the azimuthal symmetry. Parameter θ, the argument of the cos function, is the angle made with the nematic director $\hat{n}$ and $f(\theta)$ is the distribution function of the molecules (this is an average orientation of the rod-like molecules).

If θ is peaked around 0 or π which are parallel or antiparallel alignments $\cos(\theta) = \pm 1$ so $S = 1$. For a perpendicular alignment, $\theta = \frac{\pi}{2}$ and $S = -\frac{1}{2}$. If the angular orientation is isotropic, the distribution function is constant and the order parameter is null as it happens in the isotropic phase.

The scalar part of the nematic order parameter can be extracted from DNMR (deuterium nuclear magnetic resonance) experiments [4]. The molecule is "deuterated" which represents the replacement of one hydrogen atom with a deuterium one. Like in [4] this was done at the second carbon position along the alkyl chain from the biphenyl rings for the 5CB liquid crystal.

1.3 Aerosil Gel - Nanocolloidal - Structure

The second part of the mixture studied in this project consists of solid particles that do not phase-separate when mixed with the liquid crystal. Instead, they bond together and exist in a suspension, forming a cluster-like shape, surrounded by the liquid crystal. This is called a colloid, the most familiar example being oily beads in mayonnaise. As a matter of fact, these types of structures are everywhere, particularly in living beings whose blood is a biological aggregate of colloidal dispersions in mostly water.

The particles with colloidal properties utilized in this project are silica beads

7 nm in diameter. In the presence of air they collect water molecules from the environment, hydrogen-bonding together. This bonding is what keeps the beads together when they are in a mixture with liquid crystals. From the manufacturing process of aerosil, the silica beads have a large probability of fusing into pairs (about 75 %) in addition to single beads. However, fused groups of more than 2 beads are very rare. When they are in a colloid formation, the beads arrange themselves in complete closed structures, but also they might leave parts "dangling" which is yet to be discovered.

In the experiment at hand, the right amount of silica beads was mixed with liquid crystals to generate six different conjugate densities (this quantity will be explained later in the body of the AC-calorimetry experiment) from 0.03 to 0.15 g cm^{-3}. The way the mixture was obtained will be presented later in Chapter 1.

1.4 AC-Calorimetry

After obtaining the substance of interest, the next step is to discuss AC Calorimetry, the technique used in this study. Alternating Current Calorimetry is a technique generally used to map out the thermal behavior of a very small quantity - about 20 mg - of any substance of interest. The sample holder mainly consists of a small silver envelope, in the shape of a cap and lid, cold-welded with In-Sb alloy. The substance under study is in between these two silver sheets, the entire active space being an almost cylindrical chamber $\sim$ 1 mm thick and approximately 10 mm in diameter. On one side of this envelope there is a heater that can deliver very precise amounts of heat, and on the other side there is a carbon-flakes thermistor which measures the temperature. The electrical resistance of the heater is in the 100 Ω range and the thermistor has a resistance of approximately 1 MΩ at 0 ^{o}C. The small cell described above is supported only by the wires of the heater inside of a copper can. In order to create a good thermal insulation from the environment the entire ensemble is enclosed within a bigger can. The inside receives heat from the outside from a large heater wrapped around the copper cylinder - this provides the overall heating. On top of this "environmental" heating, the substance of interest will receive the AC heat. The physics of the process of heat

transfer can be expressed with equations that follow [10]:

$$C_h\dot{T} = \dot{Q}_h = \dot{Q}_o(cos\frac{1}{2}\omega t)^2 - K_h(T_h - T_s) \tag{1.3}$$

$$C_s\dot{T}_s = \dot{Q}_s = K_h(T_h - T_s) - K_b(T_s - T_b) - K_\theta(T_s - T_\theta) \tag{1.4}$$

$$C_\theta\dot{T}_\theta = \dot{Q}_\theta = K_\theta(T_s - T_\theta) \tag{1.5}$$

Here C_s are the heat capacity, K_s are the thermal conductance, and $\dot{Q}$ is the heat transfer per unit time of the :heater(h), sample(s), and thermometer (θ). The index "b" stands for bath which stands for the environment . The thermal conductivities can be considered small so the steady-state solution for T_θ of this system of equations is made of one constant term that depends upon K_b and a second oscillatory one which is inversely proportional to the heat capacity of the sample as follows:

$$T_\theta = T_b + \frac{1}{2}\dot{Q}_o\{K_b^{-1} + (1-\delta)(\omega C)^{-1}cos(\omega t - \alpha)\}$$

where $C = C_s + C_\theta + C_h$

The expression $(1-\delta)$ has a very complicated form which can be found exactly in [10] and here one must introduce the following notations:

$$\tau_s = C/K_b$$

$$\tau_\theta = C_\theta/K_\theta$$

$$\tau_h = C_h/K_h$$

where: τ are relaxation times.

The heat capacity of the sample is much bigger than the combined heat capacities of the heater and the thermometer. Another good approximation is that the relaxation time of the sample is much smaller than the one of the applied heating power. These combined assumptions give the following formulae:

$$1 - \delta = [1 + \frac{1}{\omega^2\tau_s^2} + \omega^2(\tau_\theta^2 + \tau_h^2)]^{-\frac{1}{2}}$$

and

$$\alpha \approx arcsin\{1 + [\frac{1}{\omega\tau_s} - \omega(\theta_\theta + \tau_h)]^2\}^{-\frac{1}{2}}$$

The system at hand for obtaining a good approximation is a slab (parallelepiped). A good solution for this is:

$$T_{AC} \cong \frac{\dot{Q}_o}{2\omega C}[1 + \frac{1}{\omega^2\tau_1^2} + \omega^2\tau_2^2]^{-\frac{1}{2}} \tag{1.6}$$

where τ_1 is a sample to bath relaxation time and τ_2 is a combined contribution relaxation time as follows:

$$\tau_2^2 = \tau_\theta^2 + \tau_h^2 + \tau_{int}^2$$

The subscripts stand for: θ for the thermometer, h for the heater and int internal relaxation time.

In our particular case the relaxation times are small so it is a very good approximation to assume that both relaxation times in Eq.1.6 will null the second and third term in parenthesis for the very small frequency that we use. Thus, the formula used to calculate the heat capacity of the sample is :

$$C = \frac{\dot{Q}_o}{2\omega T_{AC}}$$

T_{AC} is the resulting amplitude of the temperature oscillations. The phase shift between the amplitude of the applied heat and the amplitude of the recorded temperature can also be measured. This shift gives the exact moment when the first order transition occurs. In order to increase precision, the measurement of the temperature was done about 2000 times over ten periods. These periods were chosen very carefully after a frequency scanning of an empty cell and it was found that should be in the range of 15 mHz. The average was used in calculating the heat capacity - the ultimate goal of the experiment. An absolute precision of approximately 10 mK can be claimed but the relative precision goes to tenths of milliKelvin, which makes the technique most suitable for mapping out very subtle transitions or shifts between different types of transitions.

The latter aspect is manifested in our experiment where for the first time due to the aforementioned precision, it was discovered that a first order transition

actually has two steps (see Ref. [7]). This contradicted previous other kinds of experiments which had indicated the presence of only one step. A feature that should be noted about the functionality of AC-calorimetry is the calibration of the thermistor with an extremely exact Platinum thermometer placed very close to it. The need for calibration is due to the fact that the thermistor value drifts significantly in time, whereas the Platinum thermometer is highly stable with the value of the resistance changing very little over a range of years. Nevertheless, the thermistor is very useful due to its very high resistance (in the MΩ range) which gives a very high precision. The technique consists of applying heating power to the cell as $P_{ac}e^{i\omega t}$ and detecting the resulting temperature oscillations having an amplitude T_{ac} and a relative phase shift between the heater and the thermometer of $\varphi \equiv \Phi + \pi/2$, where Φ is the absolute phase shift between $T_{ac}(\omega)$ and the input power. The specific heat at a heating frequency ω is given by

$$C_p = \frac{[C'_{filled} - C_{empty}]}{m_{sample}} = \frac{P_{ac}cos\varphi/\omega|T_{ac}| - C_{empty}}{m_{sample}} \ , \tag{1.7}$$

$$C''_{filled} = \frac{P_{ac}}{\omega|T_{ac}|}sin\varphi - \frac{1}{\omega R} \ , \tag{1.8}$$

The equations used to extract the specific heat are Eq.1.7 and Eq.1.8. The latter is actually giving a hint in the heat transfer situation, so the usage is only to determine the exact point where the first order transition is starting, otherwise regarded as the "signature" of the isotropic to nematic transition.

1.5 Experiment

The nano-colloidal mixture described here is between 8CB liquid crystal and type 300 aerosil (the specific surface area is 300 m^2g^{-1}). The liquid crystal was synthesized at Frinton Laboratories Inc. (molar mass 291.44 g mol^{-1}). The chemical, structural formula is presented in Fig. 1.3. The "tail" has the chemical formula C_8H_{17} and it generates a lot of the subtle features of the liquid crystal due to a permanent magnetic dipole. The molecules align along the magnetic field.

The aerosil consists of $\sim$ 7 nm bids of SiO_2 that are hydrogen bonded, fact that arranges them in a colloidal structure (see Ref. [36] for more details). The

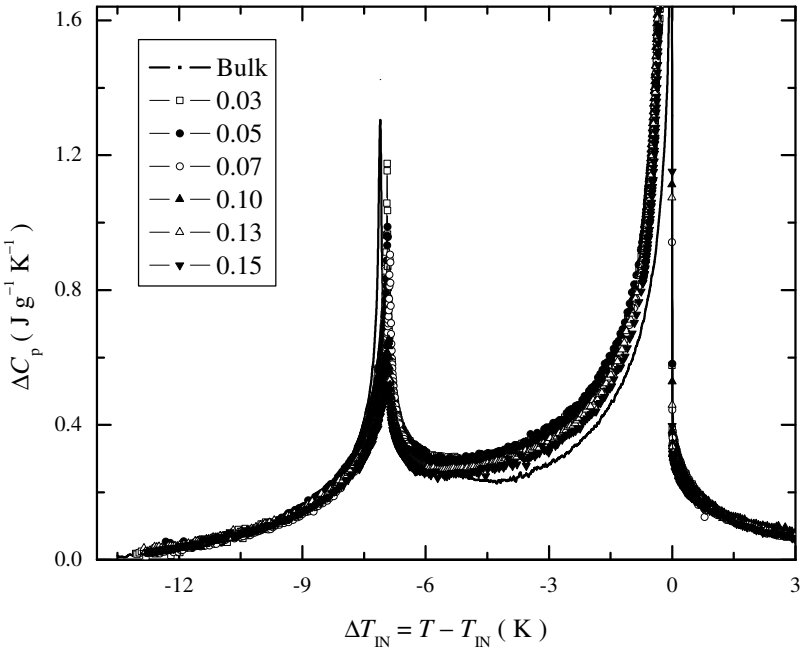

Figure 1.1. Expanded overview of the specific heat for a bulk and aligned 8CB+sil samples over $\sim$ 20 K range. Note that the wing of the I-N transition continues even "under" the N-SmA transition. The details of the I-N transition peak will be discussed later.

calorimetric measurements were done with high performance home-built calorimeters at WPI. We have prepared 6 different densities of silica in 8CB liquid crystal by adding silica powder in the liquid crystal together with acetone. After that the mixture was sonicated in the ultrasound shaker to get an uniform dispersion. At the end, the mixture underwent a forced process of evaporation of the acetone at 338.15 K and 10^{-3} Torr for about 6 hours. This last procedure was only to extract the last traces of acetone, the most of it left the mixture during the sonication. The outcome was a series of homogeneous - at least by eye inspection - samples ranging from 0.03 to 0.15 in units of g cm^{-3}, mass of silica per volume of liquid crystal.

After preparing these batches we encapsulated a quantity of $\sim$ 25 mg of each of them in between 2 foils of silver shaped as a cup and a lid, sealed together with tin in a cold welding procedure. To every one of these samples a heater and a thermistor thermometer were attached. The first was used to apply the AC

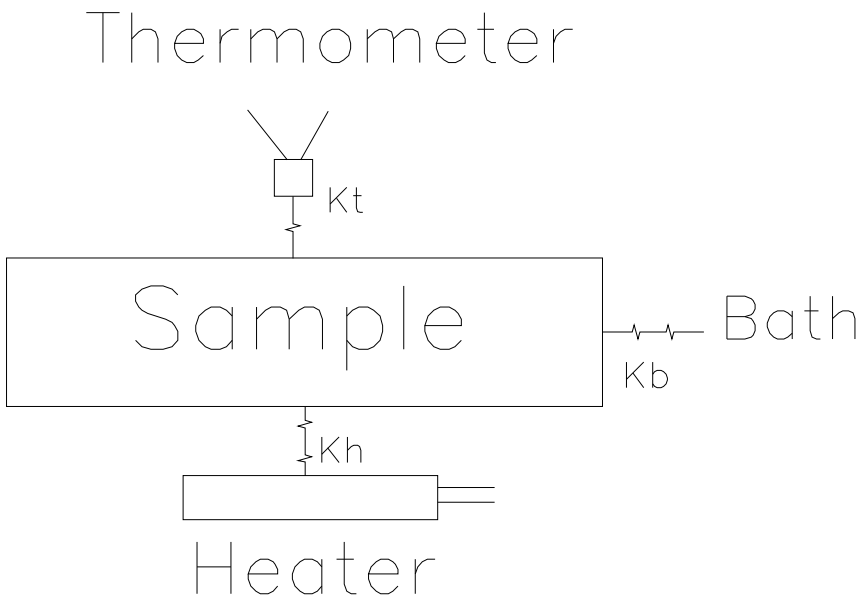

Figure 1.2. Cartoon depicting the general model of the experimental cell. Here, Kt is the thermal conductance linking the cell thermometer to the sample, Kh is the link of the heater to the sample, and Kb is the total thermal conductance of the sample+cell+thermometer+heater package to a thermal bath. Typically, $Kh \simeq Kt \gg Kb$.

heating and the second to measure the temperature of the sample. The mass of the thermometer was less then 1 mg which produces a measurement that is free of thermometrical error.

All 6 samples were exposed to a magnetic field at the Department of Physics and Astronomy, John Hopkins University, Baltimore. That consisted of cycling the samples in between nematic and isotropic phases in the presence of a very intense magnetic field. The number of cycles were at least 100 and the intensity of the field was 2 T. The temperature range of this cycling was from 308 K to 319 K with a cooling or heating rate of ~ 1 K/min. The number of cycles were necessary to obtain a robust and uniform alignment of the nematic state in 8CB+sil.

After this treatment, the samples underwent the AC calorimetric measurements at WPI together with 2 unexposed to magnetic field samples from the same batch as the aligned ones.

The experiments presented in this thesis were performed at the WPI Physics

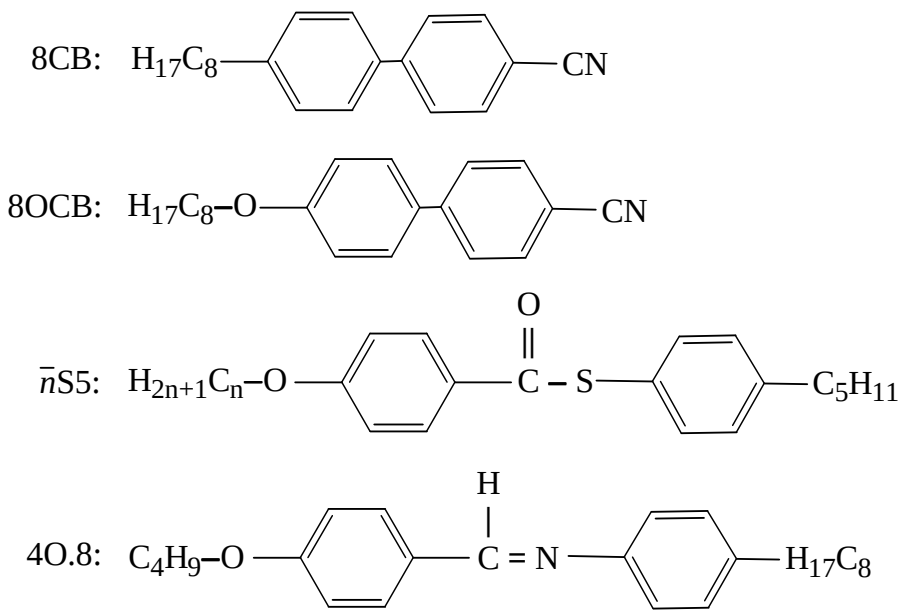

Figure 1.3. Chemical structure of some common thermotropic liquid crystals. The liquid crystal used in this work is octylcyanobiphenyl (8CB).

Department in the laboratory of Professor Germano Iannacchione. In addition, the work of our collaborators, Dennis Liang and Robert L. Leheny, served as an invaluable tool. The experiments revolved around the study of a colloidal mixture of liquid crystal and silica performed by the means of AC calorimetry. The graphical curves obtained from these experiments were interpreted with a mathematical model, allowing us to empirically find a function that best scales the specific heat of the colloidal mixture during the transition between the isotropic and the nematic phase. Later we used a power law in fitting of the second order transition.

Chapter 2

THE ISOTROPIC TO NEMATIC PHASE TRANSITION

The first chapter deals with the first order transition. In general, the specific heat features of the I-N transition in aligned (anisotropic) gel samples are consistent with those seen in random (isotropic) gel samples, namely the observance of two C_p peaks and non-monotonic transition temperature shifts with increasing silica concentration. These results reflect the scalar nature of the specific heat. However, deviations are noted in the larger transition temperature shifts with silica density as well as modification of the phase conversion process in the two-phase coexistence region for the aligned samples. Specifically and especially at lower silica densities, the lower-temperature aligned C_p peak is larger and broader while exhibiting less dispersion than the equivalent peak for the random gel. The modification of the two C_p peaks may be a consequence of the alignment altering the random-dilution to random-field crossover. While the exact origin of the larger transition temperature-shifts for the aligned samples is uncertain, the general non-monotonic behavior is interpreted using dimensional analysis as a combination of an effective elastic stiffening of the liquid crystal, combined with a liquid crystal and aerosil surface interaction energy.

2.1 Introduction to Nematics

Due to the wide variety of effects encountered, the study of quenched random disorder on phase structure and transitions is an important area that continues to attract a great deal of research activity. Of particular interest is the phase ordering of complex-fluids or soft-systems in the presence of quenched random disorder. In general, phase transitions are profoundly modified depending on the order of the transition, the character of the order affected by the disorder, the dimensionality, and the number of components of the order parameter. A great deal of progress has been made using liquid crystals (LC) as the host material and a variety of porous media as the mechanism to introduce quenched random disorder (QRD).

A particularly useful physical model is the LC+aerosil system where the QRD is created by a dispersed gel of aerosil particles and is varied by changing the density of aerosils in the dispersion. The aerosil, consisting of nanometer-size silica spheres capable of hydrogen bonding together, forms a fractal-like random gel. Numerous studies have previously been carried out by various groups on LC+aerosil [19] and the related LC+aerogel system [37]. Aerogels are self-supporting structures, which places a lower limit on the disorder strength that can be probed. However, the aerosil gel provides a weaker and more easily controlled perturbation, and thus opens up a wider range of physically interesting regimes.

The most thoroughly studied LC+aerosil system is the dispersion of type-300 aerosil in octylcyanobiphenyl (8CB), denoted 8CB+sil. Detailed calorimetric [36, 7, 24], x-ray scattering [25, 26], x-ray intensity fluctuation spectroscopy [27, 45], static and dynamic light-scattering [21, 22, 23], and deuterium NMR [28] studies on the nematic to smectic-A (N-SmA) and the isotropic to nematic (I-N) phase transitions of this system have shown that there are clear quenched random-field characteristics as well as finite-size scaling effects [19]. In what follows, a convenient measure of the introduced disorder is the grams of silica per cm^3 of liquid-crystal, denoted the conjugate silica density ρ_S, which is directly related to the surface area of solids as well as the mean-distance between solid surfaces [7]. The units of ρ_S will be dropped hereafter.

The effect of the anisotropy of the quenched disorder on the weak first-order I-N transition is studied by preparing reasonably well orientationally-aligned samples

by repeated thermal cycling through the transition in the presence of an external magnetic field. The effect of the aerosil gel network on the orientational order of the nematic phase is two-fold. The silica gel firstly dilutes the liquid crystal and secondly creates a preferred local orientation [34]. However, when the random gel responsible for the imposing of this random-field effect is strained, i.e. the gel takes on some anisotropy, a quasi-long-range ordered anisotropic nematic state is predicted [18]. This is analogous to a similar situation for smectic ordering where disorder anisotropy may lead to a smectic "Bragg-glass" phase [11, 12, 13, 14]. Some experimental evidence supporting this has recently been found by a high-resolution x-ray study of smectic ordering in aligned 8CB+sil samples [16]. The present calorimetric work is stimulated by the x-ray study but focuses on the I-N transition of aligned 8CB+sil. The results of a high-resolution calorimetric study on the smectic ordering in aligned 8CB+sil samples will be presented in the next chapter.

In general, the specific heat signatures of the I-N transition in aligned 8CB+sil samples are found to be consistent with previous measurements on unaligned, random or isotropic disordered, 8CB+sil samples [19]. The anisotropy only subtly affected the shape of the $C_p(T)$ variation near the transition, where the double specific heat peaks are signatures characteristic of LC+sil systems with $\rho_S \leq 0.1$. This double-peak feature has recently been explained as a cross-over from random-dilution dominated to a random-field dominated I to N phase conversion [29]. The general anisotropy independence of the specific heat features is simply the consequence of the scalar nature of energy fluctuations. A more significant departure from previous observation due to the imposed alignment appears in the larger magnitude of the transition temperature shift as a function of ρ_S for the aligned system. The counter-intuitive result of an aligned 8CB+sil sample being more disordered (lower T_{IN}) relative to the unaligned samples, despite having presumably quasi-long-range nematic order, may be the result of larger nematic domains encompassing more disorder sites. An empirical modeling of the effective specific heat in the I+N coexistence region has been developed in order to extract the disorder dependence of the low and high temperature specific heat peaks. This analysis indicates that the distribution of the random-dilution and random-field disorder effects are normal with little coupling between them. In addition, the

low-temperature, random-field dominated, peak is essentially constant over the range of ρ_S studied while the high-temperature, random-dilution dominated, peak decays rapidly with increasing aerosil density, disappearing at $\rho_S \sim 0.13$. Finally, a dimensional analysis of the transition temperature shift has been done. The analysis yields a consistent scaling for a variety of disordering porous media and may indicate that the interplay of surface interaction energy and effective elasticity of the host fluid is modified by these colloidal dispersions.

Section 2.2 describes the preparation of the 8CB and aerosil dispersion samples in the random and aligned states as well as the ac-calorimetry technique employed. Section 2.3 presents an overview of the calorimetric results. These results are discussed in Section 2.4, with emphasis on the C_p doubling near the I-N transition and the non-monotonic transition temperature shifts as a function of ρ_S. The conclusions are summarized in Section 2.5.

2.2 Sample Preparation and Calorimetry

Nano-colloidal mixtures of the LC+sil samples were prepared using the solvent-dispersion method [7]. The liquid crystal octylcyanobiphenyl (8CB, obtained from Frinton Laboratories Inc. and having a molar mass of 291.44 g mol^{-1}) and the hydrophilic type-300 aerosil (sil, obtained from DeGussa, Inc. having 7-nm diameter particles and 300 m^{2}g^{-1} specific area) were prepared after thorough degassing at high temperature and under vacuum for at least 2 hr. After dispersing measured amounts of 8CB+sil in high-purity (ultra low-water) acetone, the solvent was allowed to evaporate slowly over several hours. The final mixture was then degassed at ~ 320 K for $2-3$ hr to ensure complete removal of the acetone. The amount of aerosil in each sample is characterized by the conjugate density, ρ_S given as the mass of solids (silica) per open volume (8CB) in units of grams per cubic centimeters, and this is a useful quantity in relating average properties of the gel [7, 19]. Six different 8CB+sil batches were made with densities ranging from $\rho_S = 0.030$ to 0.150. The resulting 8CB+sil has a dispersed aerosil gel structure that is fractal in character over a range of length-scales [7, 45] and is termed here as a "random sample".

The aligned samples, made from the same batch of 8CB+sil, were obtained by

thermally cycling a given mixture in a sealed calorimeter cell ~ 100 times through the I-N phase transition in the presence of a 2 T magnetic field. The resulting aligned 8CB+sil samples were robust and of good quality as confirmed by x-ray studies of nearly identically prepared samples [16]. The x-ray studies also found that the aerosil gel scattering was nearly independent of the alignment procedure, which indicates that the alignment is maintained by a rearrangement of the aerosil gel on very long length-scales and the gel remains random locally [16]. It may be expected that the large length-scales of nematic (director) ordering might be affected by the alignment, which is the focus of this chapter.

High-resolution AC-calorimetry was performed using a home-built calorimeter whose basic characteristics have been described in the introductory chapter as well as in [33]. The data that have been reported in this part of the presentation were obtained by heating, because we considered that the overheating can be done only purposely unlike the overcooling. Nevertheless, the results in cooling are as close as ~ 50 mK from those in heating without showing any different features. The temperature range was between 319 and 300 K and the rate was 50 mK hour^{-1} for ± 1.5 K around the heat capacity peaks and of 400 mK hour^{-1} over the rest of the range.

The results obtained were scaled with those of the 1998 Iannacchione *et al* paper [7]. The current analysis focuses on the second order transition of the 8CB+silica for which we have a parallel study of the transition temperature, enthalpy per unit mass released in the process, and the behavior of the critical parameter α_{eff}. The above values for the 6 aligned densities are displayed in the same graph with the two unaligned densities we studied and the homologous from the 1998 above mentioned paper.

In Eqs.(1.7) and (1.8) where C'_{filled} and C''_{filled} are the real and imaginary components of the heat capacity, C_{empty} is the heat capacity of the cell and silica, m_{sample} is the mass in grams of the liquid crystal (the total mass of the 8CB+sil sample was ~ 15 mg, which yielded m_{sample} values in the range of $10-15$ mg), and R is the thermal resistance between the cell and the bath (typically 200 K W^{-1}). Equations (1.7) and (1.8) require a small correction to account for the finite internal thermal resistance compared to R. This was applied to all samples studied here [49]. Measurements were conducted at various frequencies in order to en-

sure the applicability of Eqs. (1.7) and (1.8) by checking that $C''_{filled} \approx 0$ through the effective N-SmA transition at T^*, and that C_p was independent of ω. All data presented here were taken at $\omega = 0.1473$ s^{-1} at a scanning rate of less than ± 200 mK h^{-1}, which yields essentially static C_p results. All 8CB+sil samples experienced the same thermal history after mounting: six hours in the isotropic phase to ensure equilibrium, then a slow cooling deep into the smectic phase before beginning the first detailed scan upon heating.

Extraction of the enthalpy behavior involves integrating the excess specific heat $\Delta C_p = C_p - C_{BG} - \delta C_{NA}$, where C_{BG} is a linear background describing the specific heat temperature dependence far above (+6 K) and below (−13 K) T_{IN} and δC_{NA} is the N-SmA excess specific heat contribution. Note that the high-temperature limit of the two-phase $I+N$ coexistence range, easily identified by the C''_p, is taken as T_{IN}. Direct integration of ΔC_p yields δH^*_{IN}, which contains only a portion of the transition latent heat [7]. Replacing the ΔC_p behavior in the $I+N$ coexistence region with a linear extrapolation between the boundary points as in Ref.[7] and then integrating, yields the fluctuation dominated "wing" enthalpy δH_{IN}. The difference $H = \delta H^*_{IN} - \delta H_{IN}$ is the effective phase conversion enthalpy observed by ac-calorimetry. In this study, the 19 K range of integration, temperature scan rates, heating frequency, and sample thermal history were all the same for all samples in order to facilitate comparisons.

2.3 Results

The specific heats for the aligned and random 8CB+sil samples far from the I-N transition are consistent with each other as well as with that measured for bulk 8CB. This is consistent with previous measurements on the 8CB+sil system [7] indicating that the anisotropy imposed by the alignment does not affect the short-range orientational fluctuations and these remain bulk-like independent of the aerosil structure. This result is not surprising given the scalar nature of energy fluctuation. In addition, this expectation has been experimentally verified by nearly identical specific heat results on mono-domain alkylcyanobiphenyls made parallel and perpendicular to the director [35, 15].

The influence of the alignment on the 8CB+sil system is seen primarily in the

C_p data in the two-phase I+N coexistence region and the transition temperature shifts. After determining the real and imaginary specific heats, a linear background was subtracted from all data as described previously [7] to determine the excess specific heat ΔC_p. Using the Eq. (1.8) divided by the sample mass, the imaginary specific heat C_p'' was also determined and used to gain insight into the energy dispersion at the transition as well as fixing the transition temperature (taken as the high-temperature point where $C_p'' \neq 0$, i.e. the high-temperature limit of the I+N coexistence). Figure 2.1 provides an overlay of ΔC_p for the six aligned 8CB+sil samples studied with ρ_S from 0.030 to 0.150 near the I-N transition. As with the random sil system, a double feature is clearly seen and this is currently understood to be marking the crossover from random-dilution to random-field dominated disorder [29]. In addition, a dramatic suppression of the dilution dominated sharper, high-temperature, ΔC_p for $\rho_S \geq 0.100$ is also seen in the aligned samples, marking the boundary between the soft and stiff gel regime [7].

To highlight the effect of alignment on the 8CB+sil system, two samples from the same mixture batch at low and high ρ_S were also studied without alignment (random) under identical experimental conditions. Comparisons between the random and aligned samples are shown in Fig. 2.2 for the $\rho_S = 0.050$ and Fig. 2.3 for the $\rho_S = 0.130$ sample. For the low density sample, alignment appears to broaden and enhance both ΔC_p transition features, while the imaginary part indicates that the lower-temperature, random-field dominated, peak is less dispersive and the width of the coexistence is nearly unchanged. For the high density sample, the excess specific heat is somewhat broadened but is largely unchanged by alignment. As with the low density comparison, the dispersive nature of the low-temperature peak is suppressed by the alignment but its width remains similar to that for the random sample. In both cases, the imaginary enthalpy (integrated area under C_p) is smaller for the aligned as compared to the random samples while the real effective enthalpy δH_{IN}^* is only somewhat larger for the low density aligned sample and is nearly identical for the pair of high density samples. Figure 2.4 indicates that the δH_{IN}^* variation as a function of ρ_S is nearly the same for the aligned and unaligned 8CB+sil samples. The ΔC_p wings far away from T_{IN} for aligned 8CB+sil samples and bulk 8CB overlap each other. Thus the wings yield an aerosil-density-independent enthalpic contribution $\delta H_{IN} = 5.5$ J g^{-1}, which is

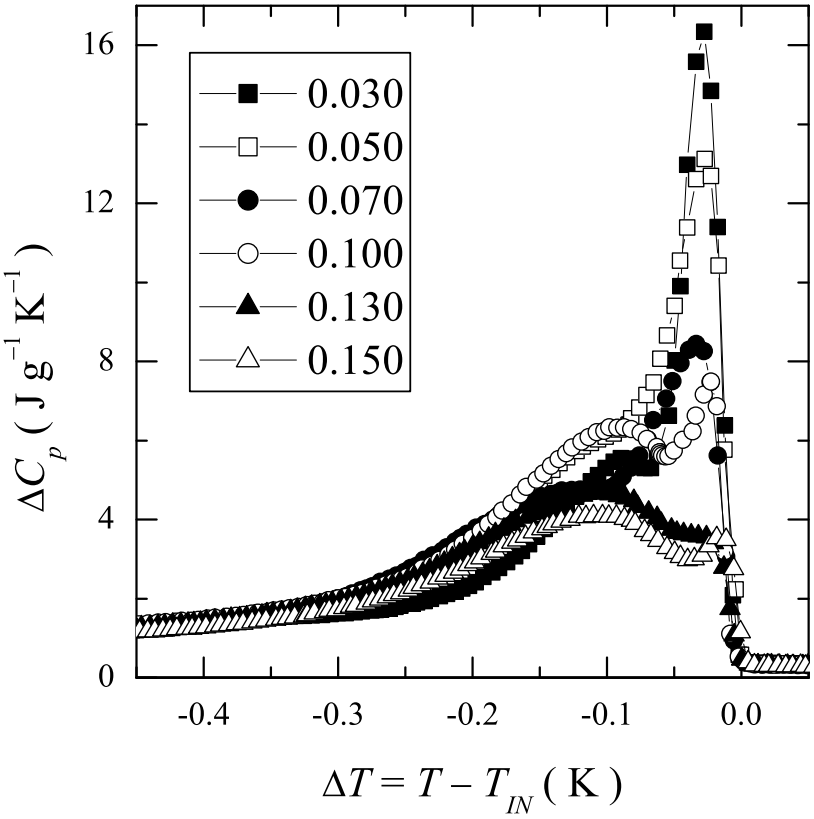

Figure 2.1. Overview of the excess specific heat near the two-phase I+N coexistence region of the I-N phase transition for the aligned 8CB+sil samples. The inset denotes the symbols for the ρ_S values of the six samples. Note that the transition temperature T_{IN} is taken as the high-temperature limit of the coexistence region.

consistent with previous measurements on unaligned 8CB+sil samples [7]. It is important to note that adiabatic calorimetry shows that the latent heat decreases with increasing ρ_S, and is expected to vanish at $\rho_S \approx 0.8$ [7, 38], far above the densities studied here. Thus, the decrease of δH^*_{IN} with increasing ρ_S is due entirely to the decrease in enthalpy in the two phase region, H, associated with the decrease in the latent heat.

While the excess specific heat is only subtly altered by alignment, and then only close to the transition, a more dramatic effect is seen in the behavior of the transition temperatures. Qualitatively, the I-N transition shifts to lower temperature as ρ_S increases in a similar manner as for the random samples. However,

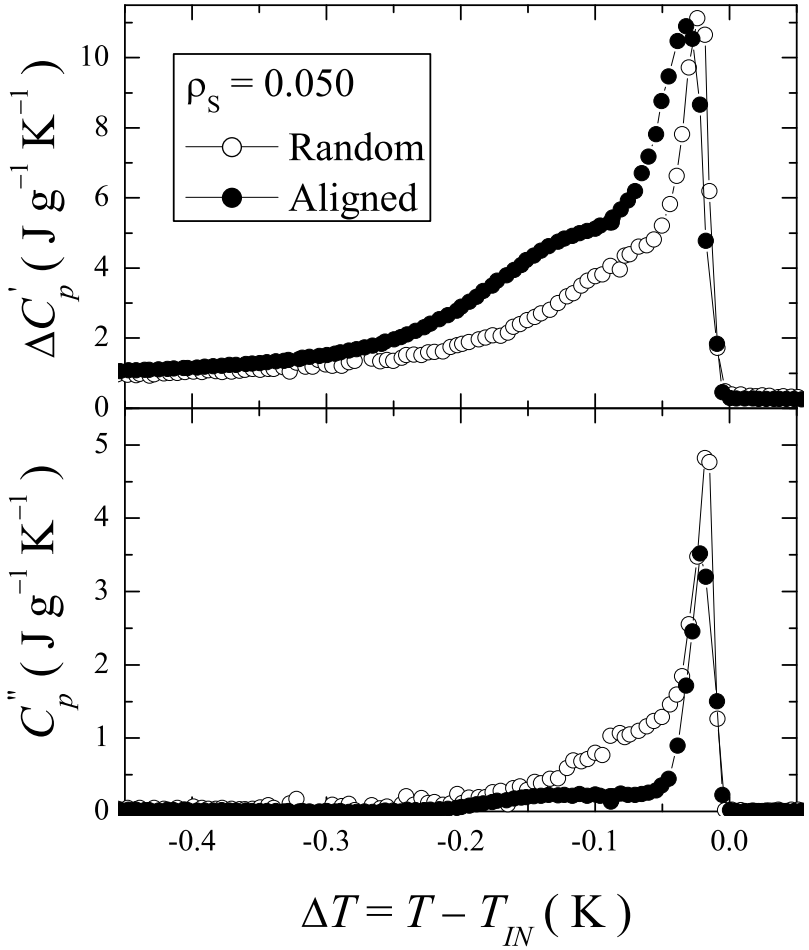

Figure 2.2. Comparison of the real excess specific heat, ΔC_p, and imaginary (dispersive) specific heat, C_p'', for the aligned and unaligned, random $\rho_S = 0.050$ 8CB+sil sample as a function of temperature near T_{IN}. Note the broadening and enhancement of the low-temperature $\Delta C_p'$ peak along with a suppression of its dispersive nature for the aligned compared to the random sample.

for all aligned samples, the magnitude of the shift with respect to the pure bulk value $\Delta T_{IN} = T_{IN}(\rho_S) - T_{IN}^{bulk}$ is ~ 0.5 K *larger*; see Figure 2.5. A comparison of the width of the nematic temperature range, shown in Fig. 2.6 for the aligned and random samples, reveals that ΔT_{nem} for aligned samples is ~ 0.2 K less than for bulk 8CB while ΔT_{nem} for unaligned samples is essentially independent of ρ_S in the range of values studied here. Finally, the isotropic+nematic coexistence range δT_{I+N}, determined by the temperature width of $C_p'' \neq 0$, for the aligned samples

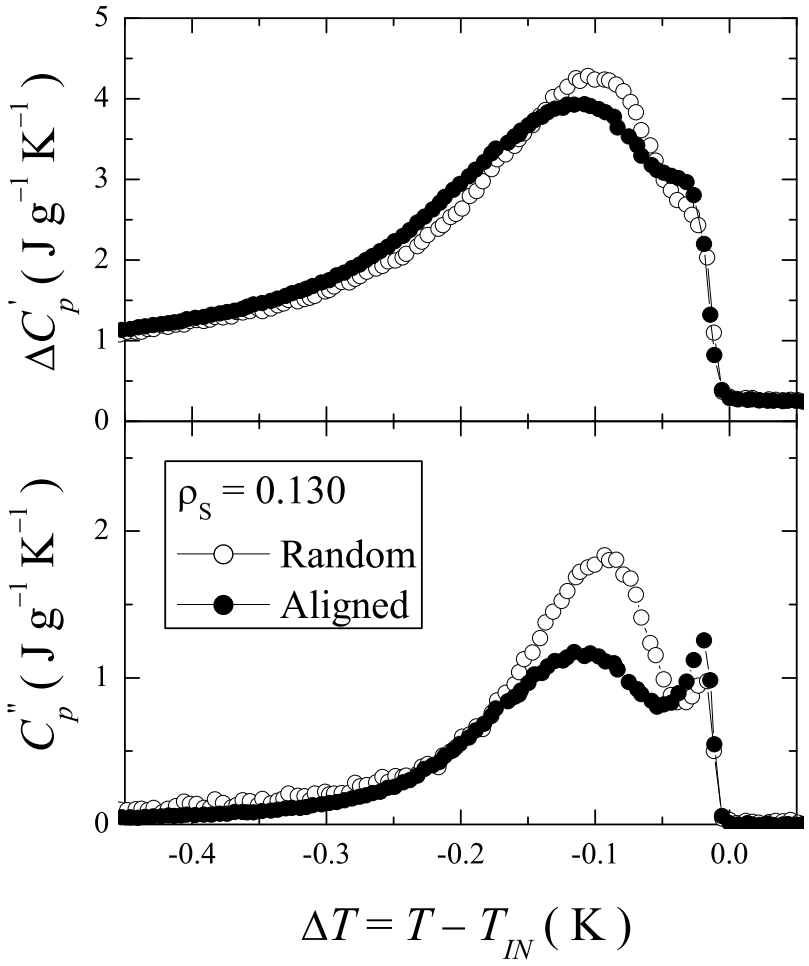

Figure 2.3. Comparison of the real excess specific heat, ΔC_p, and imaginary (dispersive) specific heat, C_p'', for the aligned and unaligned, random $\rho_S = 0.130$ 8CB+sil sample as a function of temperature near T_{IN}. Note the slight broadening of the low-temperature $\Delta C_p'$ peak along with a partial suppression of its dispersive nature for the aligned compared to the random sample.

is essentially identical to that for random samples as seen in Fig. 2.7.

Despite 8CB being a relatively stable compound, the alignment procedure requiring the 8CB+sil samples to be thermal-cycled many times into the isotropic phase may account for some of the larger transition shifts relative to the more gently handled unaligned 8CB+sil samples. However, it seems that this cannot account for all of the observed shift as sample degradation would be expected to affect both the I-N and the N-SmA roughly equally, which is not observed. Also,

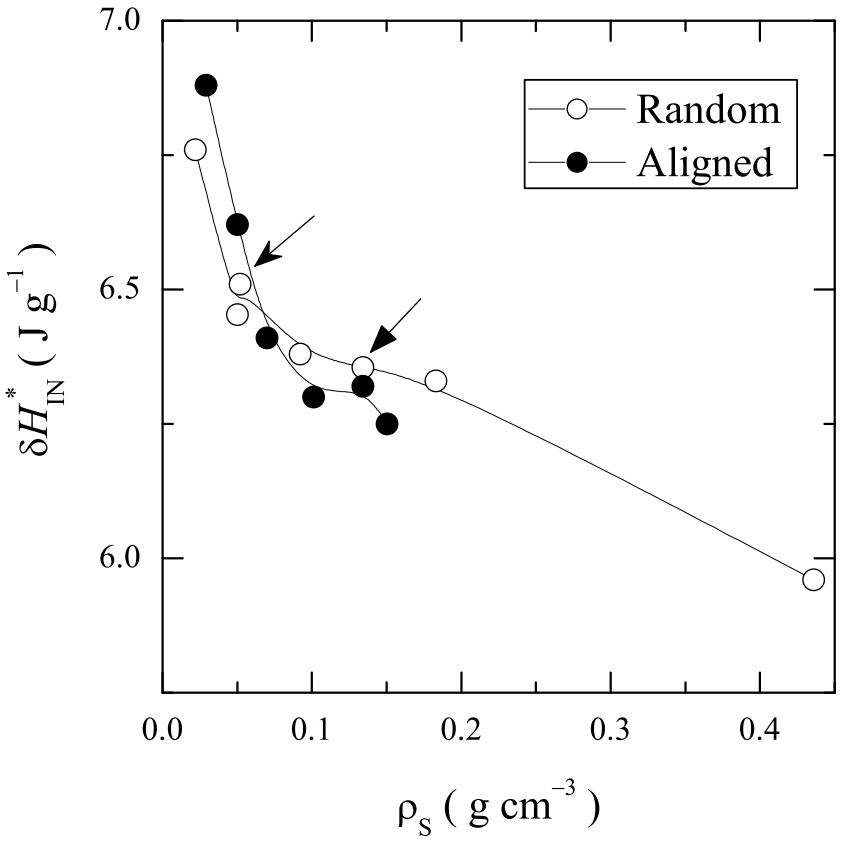

Figure 2.4. Effective integrated enthalpy δH^*_{IN}, for the aligned and unaligned, random (from Ref. [7] + two from this study indicated by the arrows) 8CB+sil samples as a function of ρ_S. These values were obtained by integrating $\Delta C_p(ac)$ from -13 K below to $+6$ K above T_{IN} with subtraction of the N-SmA contribution [7]. Due to ambiguities in the choice of backgrounds, the uncertainties are ~ 10 %. Note that the variation of this effective enthalpy with ρ_S is essentially independent of the alignment. The pointed values are from the same bottle as the aligned ones.

the coexistence width δT_{I+N}, which should be quite sensitive to the quality of the LC, appears to be unaffected by the thermal cycling. If the alignment is imprinted on the aerosil gel at only long length scales [16] and the local aerosil gel distribution remains unchanged, then the larger transition temperature shifts for the aligned samples may be the result of the larger nematic domains encompassing more aerosil gel (disorder). Table 2.1 summarizes the transition temperatures, nematic temperature range, width of the two-phase coexistence, and the effective enthalpy for the I-N transition in six aligned and two unaligned (random) 8CB+sil

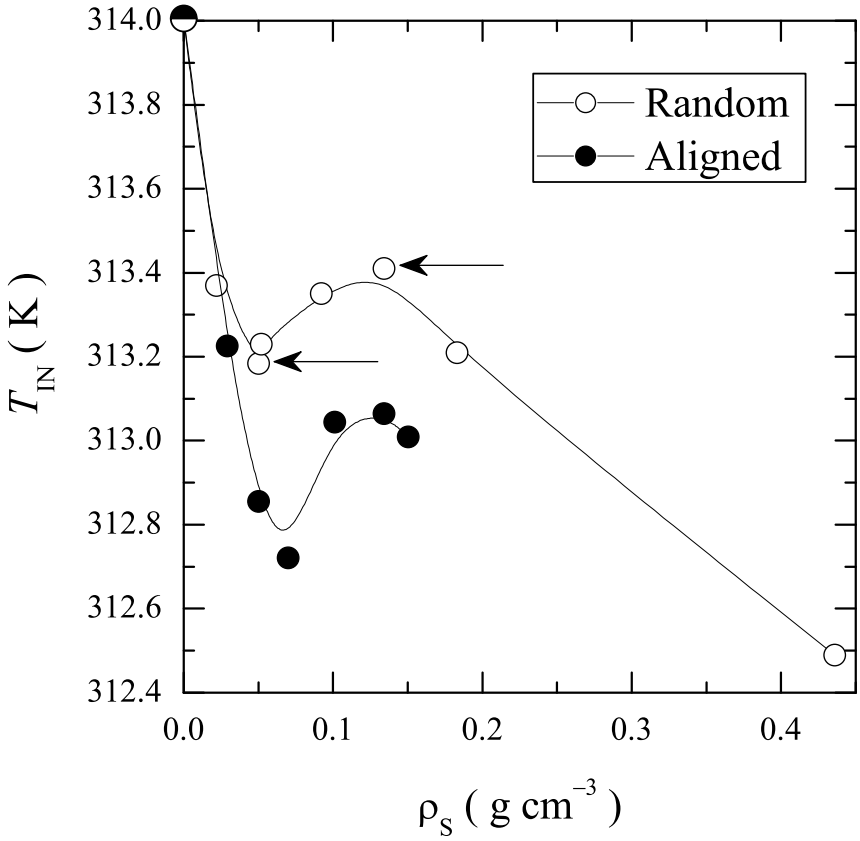

Figure 2.5. The isotropic to nematic phase transition temperature T_{IN} for the aligned and unaligned, random (from Ref. [7] + two from this study indicated by the arrows) 8CB+sil samples as a function of ρ_S. The uncertainties in T_{IN}, taken as lowest stable isotropic temperature, is ≈ 6 mK. Note the similar dependence but larger shift with ρ_S for aligned samples.

samples studied.

2.4 Discussion of the *I-N* Transition

2.4.1 Partitioning of the *I-N* Double-C_p Peak

The most striking effect of an aerosil gel on the I-N transition for both the aligned and unaligned (random) samples is the appearance of two closely-spaced transition features [7, 52, 24, 38, 39, 43, 29, 42, 44]. This effect is especially pronounced in

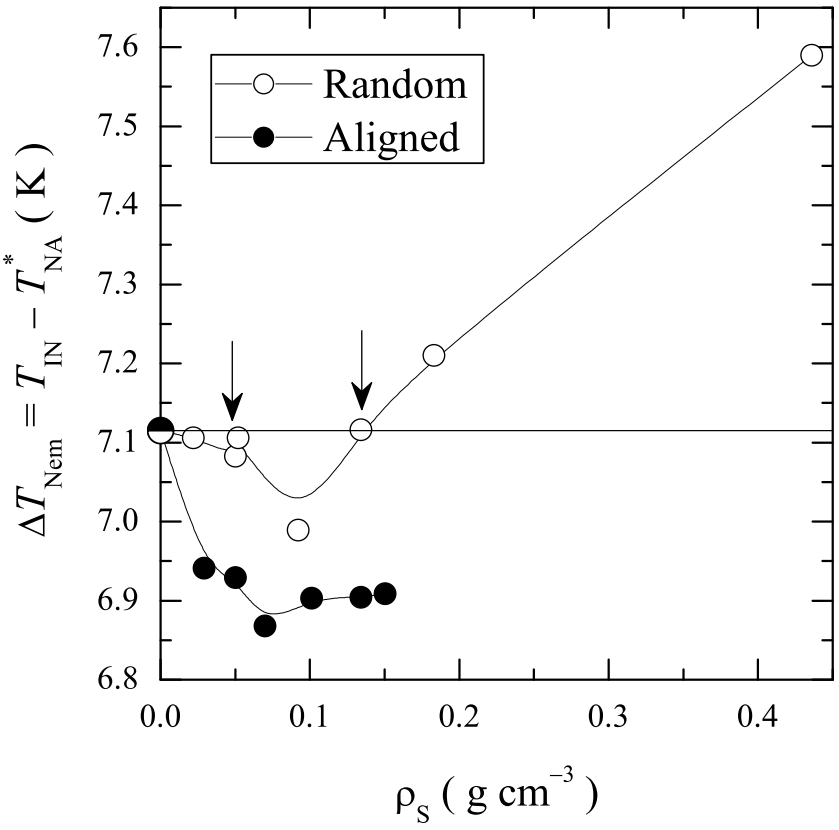

Figure 2.6. The nematic temperature range, $\Delta T_{Nem} = T_{IN} - T^*_{NA}$, for the aligned and unaligned, random (from Ref. [7] + two from this study indicated by the arrows) 8CB+sil samples as a function of ρ_S. Note the narrowing of ΔT_{Nem} for the aligned samples.

the heat capacity data. This phenomena is understood as a consequence of the soft-systems exhibiting a temperature-dependent disorder strength near the transition which results in a crossover from random-dilution to random-field effects [29]. The results of the present study are completely consistent with the literature and indicate only minor modification to the distribution of dilution and field effects for aligned samples.

To better quantify the partition between the high-temperature, dilution dominated, and the lower-temperature, random-field dominated, *I*-*N* C_p peaks, a fit was performed on these peaks over a narrow range of temperatures capturing the entire two-phase coexistence region. The functional form to be used assumes that

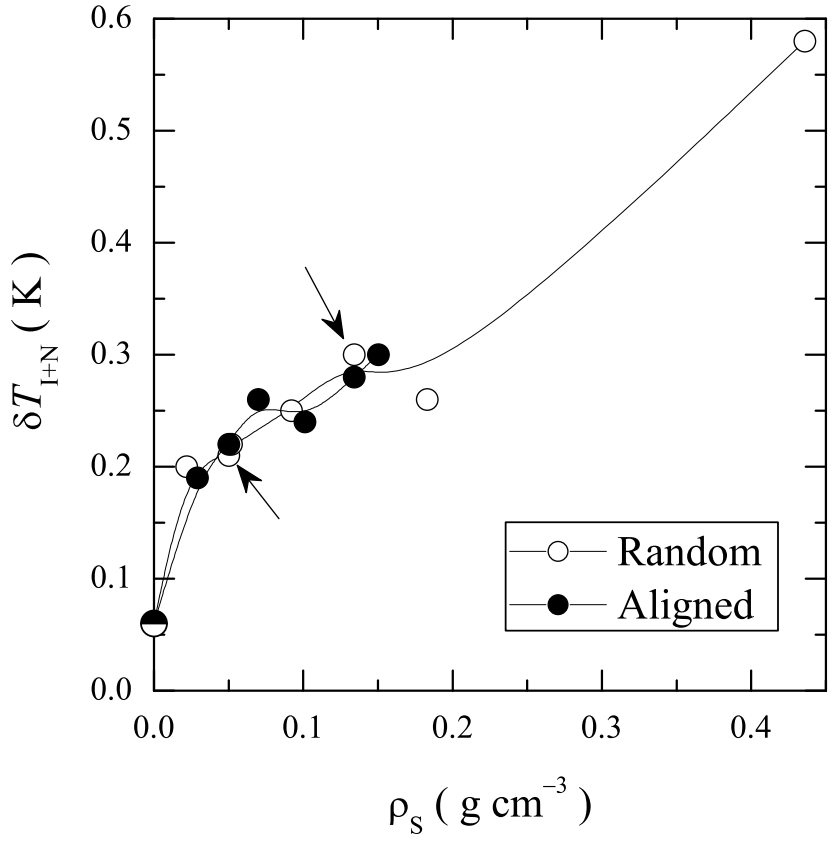

Figure 2.7. The isotropic+nematic coexistence temperature range, δT_{I+N}, for the aligned and unaligned, random (from Ref. [7] + two from this study indicated by the arrows) 8CB+sil samples as a function of ρ_S. As determined by the width of the dispersion (imaginary) C_p'' peak, δT_{I+N} has an uncertainty of ~ 20 mK. Note that the coexistence width is insensitive to the alignment.

the $I+N$ coexistence at the transition in LC+sil systems consists of two processes that each obey a normal statistical distribution and are essentially independent. These assumptions naturally lead to a form that consists of the superposition of two Gaussian terms such as

$$\Delta C_p = \frac{a_1}{\sigma_1} \exp\left(-\frac{(\Delta T - \mu_1)^2}{2\sigma_1^2}\right) + \frac{a_2}{\sigma_2} \exp\left(-\frac{(\Delta T - \mu_2)^2}{2\sigma_2^2}\right), \qquad (2.1)$$

where the subscripts 1 and 2 denote the high and low temperature peaks; respectively, ΔC_p is the excess specific heat, $\Delta T = T - T_{IN}$ is the distance from

Table 2.1. Summary of the calorimetric results for the isotropic to nematic phase transition in the six aligned and two unaligned 8CB+sil samples. The units for conjugate aerosil density ρ_S are grams of aerosil per cm^3 8CB; the transition temperature T_{IN}, nematic range ΔT_{Nem}, and coexistence width δT_{I+N} are Kelvin; effective ac-enthalpy δH^*_{IN} and the contribution of the high-temperature peak h_1 and low-temperature peak h_2 effective enthalpies are are in Joule per gram 8CB (see text for details). For all parameters, the uncertainties are ± 2 in the last digit except for δH^*_{IN}, which is ± 0.05 and the effective enthalpies h_1 and h_2 has the $\sim 10\%$ error that had been mentioned.

Sample	ρ_S	T_{IN}	ΔT_{Nem}	δT_{I+N}	δH^*_{IN}	h_1	h_2
Aligned	0.030	313.226	6.941	0.19	6.88	0.62	0.83
	0.050	312.855	6.929	0.22	6.62	0.39	0.80
	0.070	312.721	6.870	0.26	6.41	0.24	0.74
	0.100	313.044	6.903	0.24	6.30	0.09	0.78
	0.130	313.064	6.904	0.28	6.32	0.01	0.88
	0.150	313.009	6.909	0.30	6.25	0.03	0.79
Unaligned	0.050	313.184	7.038	0.21	6.45	0.34	0.78
	0.130	313.410	7.116	0.30	6.36	0.12	0.90

the transition temperature, σ_i, μ_i, and a_i are the standard normal distribution parameters describing the width, center (relative to T_{IN}), and amplitude of each distribution (process). The application of Eq. (2.1) requires it to be truncated at the high-temperature limit of the coexistence region. A more realistic expression would be required to go to zero at this limit and so, take on a distorted Gaussian form. However, this refinement seems unnecessary given the purpose of the present exercise. It should be stressed that this empirical form does not represent any theory but is only a means of characterizing the partition of the enthalpy between the random-dilution and random-field effects. In addition, the integration of the ac-determined ΔC_p would yield only an effective enthalpy that includes part but not all of the first-order latent heat (see Section 2.2 and Ref. [7]). However, all measurements in this study were conducted under identical experimental conditions, thus the effect of both alignment and aerosil density should be isolated by this analysis as a proxy for a more detailed experimental measurement of the true total transition enthalpy.

An example of the application of Eq. (2.1) to the ΔC_p data through the $I+N$

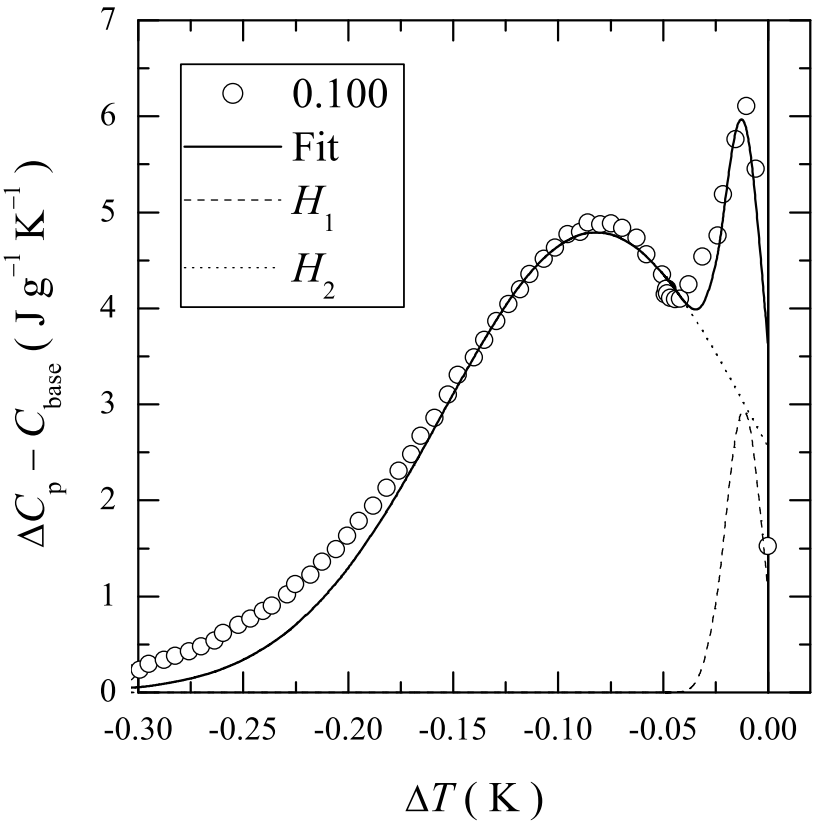

Figure 2.8. Fit (solid line) using the two-Gaussian model given by Eq. 2.1 to the excess specific heat over the entire two-phase (I+N) coexistence region of the $\rho_S = 0.100$ aligned 8CB+sil sample. Dashed and dotted lines indicate the contributions of the low-temperature (H_1) and high-temperature (H_2) peaks, respectively. See inset. Note that the fit must be truncated at the high-temperature limit of the coexistence region and that a constant baseline value was subtracted. Fits made to the other samples were of similar quality.

coexistence region is shown in Fig. 2.8. Similar quality fits were obtained for all aligned and unaligned samples studied. The fits suggest that the distribution of phase conversion in the presence of each effect, random dilution, and field, is nearly normal and so, represent independent events. That is, the nematic conversion of either a dilution or field dominated domain is not coupled strongly to a neighboring domain's conversion.

From the fit results, the area for each term (each truncated at the high-temperature limit of the coexistence range) H_1 and H_2, respectively, can be calcu-

lated. However, as seen in Fig. 2.8 and similarly for all such fits, Eq. (2.1) fails to model the peak farther than about 0.2 K from T_{IN} and so the total integration of Eq. (2.1) would not yield the correct H as obtained experimentally. By assuming that the ratio of each term's area, $R \equiv H_1/H_2$ is close to being correct and taking the measured H, a reasonable estimate of each peak's area may be calculated by $h_1 = RH/(1+R)$ and $h_2 = H/(1+R)$ for the high and low temperature peaks, respectively (with $h_1 + h_2 \equiv H$). The uncertainties in h_1 and h_2, which are ~ 10 %, are due to the fitting while the uncertainty in H is typically ± 0.05 J g^{-1} and the results are listed in Table 2.1 for all samples studied. Comparison of the h_1 and h_2 contributions for the random and aligned samples with $\rho_S = 0.050$ indicates that despite the obvious broadening seen in Fig. 2.2 for the aligned sample, the relative contributions of dilution and field effects remains unchanged. However, for the sample with $\rho_S = 0.130$, there is a significant increase in the random-dilution contribution to the transition enthalpy for the aligned sample.

A plot of the ρ_S dependence of the peak areas h_1 and h_2 is shown in Fig. 2.9. The low-temperature, random-field dominated, effective enthalpy h_2 is effectively constant through this low range of aerosil densities, while the high-temperature, random-dilution dominated, effective enthalpy h_1 decreases rapidly with ρ_S, mirroring the decrease of the total effective enthalpy H, until it essentially vanishes at $\rho_S \approx 0.13$. Although this can be inferred from the behavior shown in Fig. 2.1, this analysis makes it clear that the decrease in the I-N transition enthalpy occurs in two stages. In the low-density range ($\rho_S \leq 0.1$), the random-dilution dominated peak decays, while the random-field dominated peak is nearly ρ_S-independent. Given the results of the wider ρ_S range studies of Refs. [7] and [38], the remaining random-field dominated peak should begin to decrease for larger ρ_S and eventually disappear at $\rho_S \approx 0.8$. Such a scenario, coupled with the temperature dependent total disorder strength of the random dilution to random field crossover [29], may be important in explaining the non-monotonic transition temperature decrease with ρ_S.

The fact that the graph of the specific heat is fitted very well with a sum of two gaussian functions, make one entitled to speculate that the quantity missing from the specific heat graph due to the imperfection of the AC-calorimetry technique might be a constant. If that was not true, then the shape of the graph would be

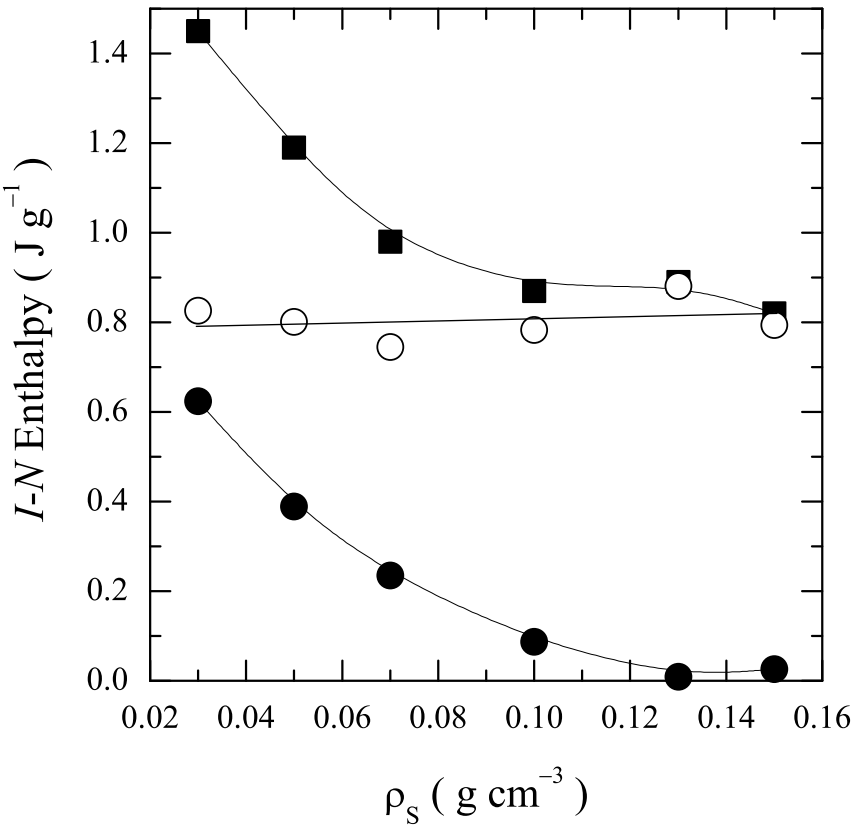

Figure 2.9. Plot of the ρ_S dependence of the random-dilution dominated high-temperature peak enthalpy h_1 (open circles), the random-field dominated, low-temperature peak, enthalpy h_2 (solid circles), and the measured coexistence area H (solid squares) for the aligned 8CB+sil samples. The solid lines are guides to the eye. Note the near constant behavior of h_2 in contrast to the rapid decrease in h_1.

distorted from a gaussian and the fit could not be reached.

2.4.2 Dimensional Analysis: ΔT_{IN}

Another striking feature of the effect of the aerosil gel on the I-N transition is the non-monotonic shift in the transition temperature, ΔT_{IN}, as shown in Fig. 2.5. Various mechanisms have been explored to account for the observed behavior such as finite-size nucleation (due to the first-order character of the I-N), elastic strain, random pinning (see Ref. [5, 7] for a discussion of these three), and more recently

an extended "single-pore" model to account for surface anchoring [40]. However, all these current models yield smoothly varying functions of confining length or disorder (silica) density and the non-monotonic behavior remains unexplained. Recently, it has been shown that the I-N transition in the presence of quenched random disorder proceeds is via a two-step process of cooling, first random-dilution and then random-field, and this successfully accounts for the doubling of the I-N transition features [29]. Further, it was speculated that this might also account for the behavior of ΔT_{IN} for these systems via the required temperature dependent disorder strength (see also Ref. [39]) but this idea remains unexplored.

The experimental observations on the behavior of the LC+sil system as a function of ρ_S, such as the evolution of the critical behavior of the N-SmA [7, 43] and ΔC_P peak shape of the SmA-SmC [44] transitions, rheological studies [16, 41], and dynamic x-ray scattering studies [27, 45], strongly suggest that the colloidal dispersion of the aerosil gel alters the effective elastic (and perhaps other material) properties of the host LC fluid.

To expand on the notion that the LC material parameters may become ρ_S dependent, a dimensional analysis may be performed on ΔT_c based on four important quantities: the effective elastic constant, $\bar{K}$ in (J m^{-1}), surface interaction energy density, W in (J m^{-2}), conjugate aerosil density, ρ_S in (Kg m^{-3}), and the transition entropy change, ΔS_c in (J K^{-1} Kg^{-1}), yielding

$$|\Delta T_c| \sim \frac{W^2}{\bar{K}\rho_S \Delta S_c} \sim \frac{W^2 T_c}{\bar{K}\rho_S \Delta H_c}, \tag{2.2}$$

where the entropy change at T_c is related to the enthalpy change (latent heat) by $\Delta H_c = T_c \Delta S_c$. Note that if the bulk value of $\bar{K}$ as well as the anchoring energy density W were assumed constant, Eq. (2.2) would also not yield the observed non-monotonic behavior of ΔT_c. However, if $\bar{K}$ and W were aerosil dependent, then this analysis could be used to shed light on the ρ_S dependence of the effective material parameters of the composite system. Equation (2.2) may be rearranged to group together the experimentally accessible quantities to give

$$\frac{|\Delta T_c|}{T_c} \Delta H_c \rho_S \sim \frac{W^2}{\bar{K}}, \tag{2.3}$$

which has units of (J m^{-3}) and can be termed the LC+QRD energy density. Accurate ac-calorimetric data are available for the liquid crystal 8CB in controlled porous glass [40], aerogel [46], random aerosil gel [7], and aligned aerosil gel of this work. However, each data set, although taken under similar ac-calorimetric experimental conditions, is missing a significant portion of the latent heat. Thus, the effective transitional enthalpies available from these studies are used only as a proxy for the true value of ΔH_{IN}.

With Eq. (2.3), the ρ_S dependence of $W^2/\bar{K}$ is found and plotted in Fig. 2.10. Given the uncertainties (primarily in estimating ΔH_{IN} from ΔH^*_{IN}), the behavior of the LC+QRD energy density is reasonably describable by a power-law, $W^2/\bar{K} \sim \rho_S^n$ where the exponent for both the low-density ($\rho_S < 0.1$) aerosil and the aerogel is $n = 1.5$ (see solid lines in Fig. 2.10). Since the low-density aerosil gel is extremely soft as compared to the aerogel (or CPG or high-density aerosil with $\rho_S > 0.1$), the non-monotonic behavior of $T_{IN}(\rho_S)$ reflects a change in the effective stiffness and anchoring of the LC to the QRD surfaces.

Given the behavior of the LC+QRD energy density, the functional dependence of W and $\bar{K}$ separately may be inferred. Using the observed power-law and the condition that as $\rho_S \to 0$, $W \to 0$ (no surfaces present) and $\bar{K} \to \bar{K}_0$ (the bare bulk liquid crystal value), suggests $W \sim \rho_S^w$ and $\bar{K} \sim \bar{K}_0 + c\rho_S^k$. Noting that the exponents n, w, and k must be positive, a relationship among them depends on the magnitude of $\bar{K}_0$ relative to the diverging part. If $\bar{K}_0$ is negligibly small, then the exponents must satisfy $2w - k = n > 0$. Otherwise, the general relation $2w - k < n < 2w$ applies. Overall, this analysis is intuitively reasonable as one would expect the composite to effectively stiffen and the random nature of the solid surfaces to trap more disorder energy as the solid's density increases.

2.5 Conclusions for the *I*-*N* Transition

This chapter presents a high-resolution calorimetric study of the effect of sil alignment on the isotropic to nematic phase transition of the quenched disordered 8CB+aerosil system. As expected, the overall specific heat signature of I-N transition in this system is weakly affected by the alignment, reflecting the scalar nature of energy fluctuation. The results are largely consistent with results on unaligned

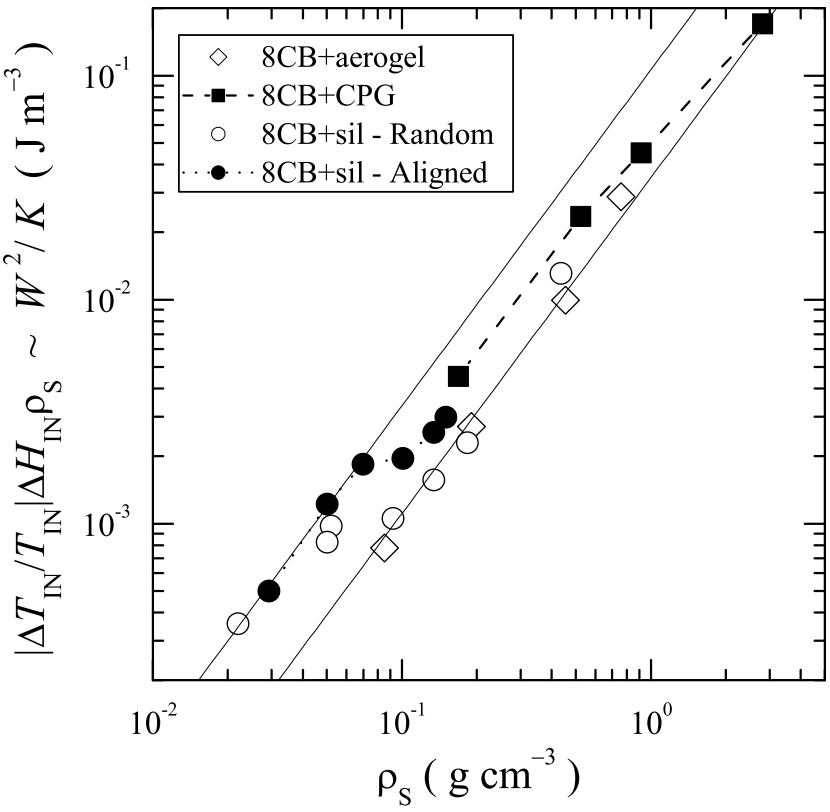

Figure 2.10. Comparison of the derived LC+QRD energy density $W^2/\bar{K}$ as a function of ρ_S for the 8CB+QRD (8CB+aerogel [46], 8CB+CPG [40], random 8CB+sil [7], and aligned 8CB+sil [this work]). See inset for symbol labels. Both solid lines indicate a power-law with an exponent of $n = 1.5$. See text for details.

(random gel) samples, again revealing as the most significant features the doubling of the I-N transition and a non-monotonic decrease in the transition temperature with aerosil density. Differences emerge in the magnitude of the transition temperature shift, being unexpectedly larger for the alignment, and small changes in the C_p peak shapes in the coexistence range. How the sil alignment causes these effects is not entirely clear but it may be related to the aligned samples having larger nematic domains and so, forced to encompass more aerosil surface (disorder). In addition, there is the possibility that the aligned aerosil gel may be stiffer than the random gel and so impose greater disorder.

An empirical analysis of the specific heat peak shapes using a two-Gaussian

model yielded the effective enthalpy contribution for the dilution-dominated and field-dominated peaks. While not containing any physics of the disorder, the decent fits indicate the normal distribution of the isotropic to nematic phase conversion under the influence of random-dilution and random-field effects with relatively little coupling. In addition, the aerosil density dependence indicates that the random-field dominated peak h_2 is nearly constant from the percolation threshold ($\rho_S \sim 0.015$) to 0.15, while the random-dilution dominated peak h_1 decays rapidly. This analysis combined with the results of Refs. [7] and [38] indicates that the decrease in the I-N transition enthalpy H determined from $C_p(ac)$ data (and presumably the total latent heat as well) occurs in two stages. As ρ_S increases, there is a rapid decrease in the random-dilution dominated contribution, which disappears at $\rho_S \cong 0.13$, and this is followed by an eventual decrease in the random-field dominated contribution when the aerosil density is increased above 0.15.

A dimensional analysis of the transition temperature shifts as a function of aerosil density resulted in a relationship that involves an effective elastic constant as well as a surface interaction energy, both of which behave as power-laws. This reflects the effective stiffening of the colloidal dispersion with increasing aerosil content. In addition, the same analysis applied to a variety of 8CB systems with quenched random disorder such as unaligned (random) aerosil gels, aerogel gels, and controlled-porous glasses, reveal a general behavior and indicate that the resulting exponents are topology independent. High-resolution latent heat measurements through the double peak feature would greatly aid the peak partition analysis as well as better refine the LC+QRD energy density estimate.

Chapter 3

THE NEMATIC TO SMECTIC-A PHASE TRANSITION

3.1 Introduction to the Nematic - Smectic-*A* Transition

3.1.1 Universality Classes

The nematic to smectic-A phase transition is a second order one. According to the Ehrenfest classification, these transitions are those which have the second order partial derivative of a thermodynamical potential discontinuous when passing from one state to another. A different way to identify a second order transition is to observe a certain extensive thermodynamical parameter having a value different from zero only in one of the two phases involved in the transition. An example would be the transition that iron undergoes at 1042 K when it transforms from a paramagnetic to a ferromagnetic state. The parameter that is non-zero only in ferromagnetic state is the spontaneous magnetization. Ehrenfest predicted a "n"-th order phase transition which has not been found experimentally. In Landau approach, there is a change in symmetry when passing from one phase to another. This imposes the existence of an "order parameter" which is non-zero in the less symmetric phase (higher order), and null in the higher symmetry phase.

The nematic to smectic-A phase transition has been given an enormous amount

of attention by the scientific world due to Pierre de Gennes theoretical approach [8] of using the very same formulae as Landau did for the normal-superconductor phase transition [9]. His approach was pretty fertile, leading to numerous publications. Another way to explain what universality class is: if one has already found a behavior in the last cited experiment, they should look for one similar in N-SmA transition. In the "vicinity" of the critical point, many important measurable quantities obey a power law whose exponents are called: *critical exponents*. These exponents have the same values for any transition that obeys a universality class, without depending on the particular field it is referred to. In conclusion, the fact that one can consider two apparently unrelated phenomena as obeying the same physical formula, is called "universality class".

3.1.2 Characteristics of the Random-Field 3D-XY Model

The model giving the closest fit between the theory and the experimental data is random-field 3D-XY. This model originated in the normal-superconductor transition. The Hamiltonian for this transition is:

$$H = J\sum_{x,y} \overrightarrow{s_x}\cdot\overrightarrow{s_y} + \sum_{x} \overrightarrow{h_x}\cdot\overrightarrow{s_x} - \sum_{x} \overrightarrow{H}\cdot\overrightarrow{s_x} \tag{3.1}$$

where $\overrightarrow{H}$ is an external field and $\overrightarrow{h_x}$ represents a local, randomly varying field, modeling the influence of the quenched disorder. The first term in Eq. (3.1) models the pure bulk 3D-XY universality class. The local random field must satisfy

$$< \overrightarrow{h}_x >_{\overrightarrow{r}} = 0; \qquad < \overrightarrow{h}_x \cdot \overrightarrow{h}_x >_{\overrightarrow{r}} = h_o^2 \tag{3.2}$$

where $<>_{\overrightarrow{r}}$ is the spatial average. The XY notation reflects that the spins can only rotate in a plan thus requiring a vector representation. For liquid crystals, the uniform external field $\overrightarrow{H}$ may be either electric or magnetic in nature while the local field $\overrightarrow{h_x}$ typically emerges from the van der Waal interactions of dispersed surfaces within the LC.

3.1.3 The de Gennes Superconductor Analog: Mean-field

The smectic-nematic phase transition was approached by deGennes [8] with an extension of the Landau theory for the order parameter. For the smectic phase, one can take as order parameter the one following in the next discussion. Because in the smectic phase the molecules form layers, the density can be expressed as:

$$\rho(\overrightarrow{r}) = \rho(z) = \rho_o + \rho_1 cos(q_S z - \Phi) \tag{3.3}$$

where z is the direction perpendicular to the layer, ρ_1 is the amplitude of the first harmonic, q_S is the amplitude of the wave vector and Φ is an arbitrary phase. The order parameter chosen by deGennes was ρ_1 which is obviously null in the nematic phase as required. With this parameter, the free energy per unit volume takes form:

$$f_s = \frac{1}{2} r \rho_1^2 + \frac{1}{4} u_o \rho_1^4 + \cdots \tag{3.4}$$

In order to introduce the layer fluctuations, one can choose a smectic order parameter of the following form:

$$\Psi(\overrightarrow{r}) = \rho_1(\overrightarrow{r}) e^{i\Phi(r)} \tag{3.5}$$

where:

$$\Phi(\overrightarrow{r}) = -q_s u(\overrightarrow{r}) \tag{3.6}$$

with $u(\overrightarrow{r})$ the layer displacement and now allowing to fluctuate and hence to depend on position. A final formula for the free energy is :

$$F_{NA} = \frac{1}{2} \int d^3x \{ r \ |\Psi|^2 + \frac{u}{2} |\Psi|^4 + C|\nabla - i q_s \delta\hat{n}_\perp \Psi|^2 + \widetilde{K_1} div^2 \delta\hat{n}_\perp + \widetilde{K_2} (\hat{z} \cdot curl \delta\hat{n}_\perp)^2 + \widetilde{K_3} (\frac{\partial}{\partial z} \delta\hat{n}_\perp)^2 .$$

As deGennes pointed out, this formula resembles very well with that of the free energy in Landau-Ginzburg theory for normal-superconductor transition:

$$F_{SC} = \frac{1}{2} \int d^3x \{ r \ |\Psi|^2 + \frac{u}{2} |\Psi|^4 + \frac{1}{m} |(\hbar\nabla - i\frac{q}{c}\mathbf{A})\Psi|^2 + \frac{1}{8\pi\mu} (curl \ \mathbf{A})^2 \} \tag{3.7}$$

Comparing these two members of the same 3D-XY universality class, there emerges the following correspondence [8]:
$\delta\hat{n}_\perp \longrightarrow \mathbf{A}$ (magnetic vector potential)
$C \longrightarrow m^{-1}$ (m mass of superconducting pair)
$q_s \longrightarrow q/c$ (charge of superconducting pair divided by the speed of light)
$K_1 \longrightarrow 1/\mu$ (μ is magnetic permittivity)
gradient of free-energy energy $\longrightarrow$ kinetic energy
Frank-Olsen elastic energy $\longrightarrow$ magnetic energy.

3.1.4 Smectic Issues

When talking about any phase transition, one can focus on two aspects: order and symmetry. Higher order is lower symmetry and *vice versa*. The pure melting process is a clear change from higher order (lower symmetry) of the solid state to a lower order (higher symmetry) of the liquid phase. For the first order, the explanation of the transition is clear. One degree of freedom is frozen (on cooling), so one loses symmetry and gains order. For the second order transition, nothing like that happens. Therefore, how can one use the same approach as they did for the first order transition? The answer is in a new category called *dynamic symmetry*. Ergo, during the second order transition a dynamic symmetry is broken. This is the reason why there is now jump in enthalpy. Intimately, in the nematic state, molecules are free to migrate (translation) while still obeying the nematic directory, whereas in the smectic phase there are layers of molecules. Even if molecules can migrate between the layers, this kind of motion is drastically limited. In conclusion, the transition from nematic to smectic can be understood as a reduction in mobility.

For a better understanding of this idea, one can observe in Fig.3.1 the behavior of a generic enthalpy in the vicinity of the phase transition. The formula used to calculate the the enthalpy was obtained by analytically integrating the formula that fits the specific heat behavior for the critical region of the smectic-nematic transition 3.11. The result of energy for one wing is:

$$H = |t|\frac{A}{1-\alpha}|t|^{-\alpha}[1 + \frac{1-\alpha}{\Delta-\alpha+1}D|t|^{\Delta}] \tag{3.8}$$

The graph was done considering D, the amplitude correction to scaling, as it should

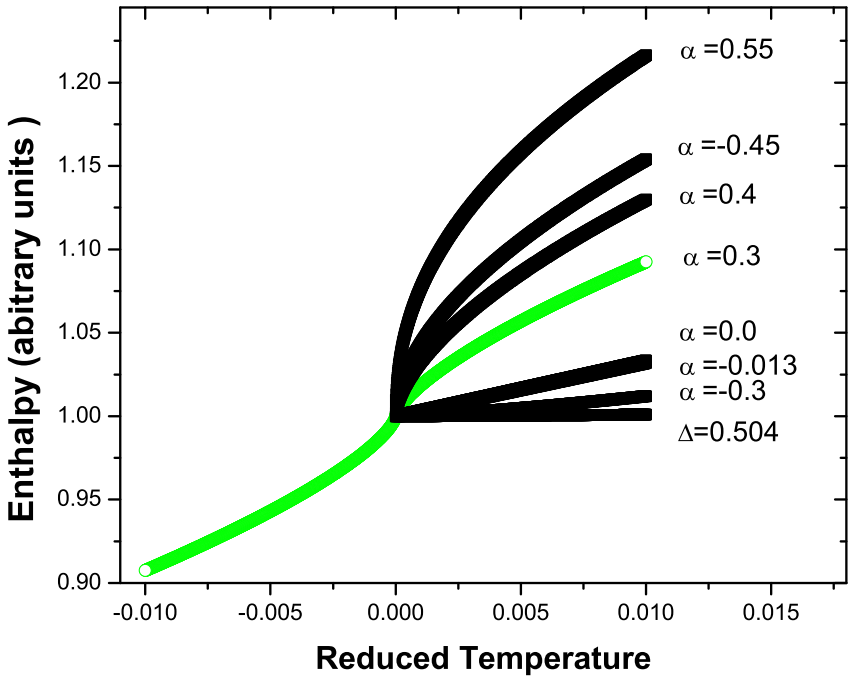

Figure 3.1. Generic behavior of enthalpy in a nematic-smectic-A phase transition. The transition in the range $\pm 10^{-2}$ in the reduced temperature is given for different values of α. For $\alpha = 0.3$ there are both sides of the of the graph. The bottom right side is an exemplification of how the correction to scaling looks like.

be, negligible comparative to A. Only the graph for $\alpha = 0.3$ was done for both before and after the critical point. One can notice the following trend: as α increases towards unity, the entrance in the critical point and the exit are steeper and steeper until, for values close to 1, it has a jump and it would become a first order transition if it was not for the limiting value $\alpha = 0.5$. Now, as critical exponent α decreases to zero, both upper and lower branches become flatter so at $\alpha = 0$, the correction to scaling becomes dominant. Nevertheless, the contribution is very flat as one can see from the lowest graph on the right hand side. Mathematically, the slope of the enthalpy changes from concave to convex at the critical point. Also, the critical exponent being negative, makes the curvature to be inverted comparative to positive α. An observation to this paragraph is that the fitting Eq. (3.11) lacks a term that depends on the density of the mixture element in the liquid

crystal in hand.

3.2 Previous Results on Quenched Random Disorder in Liquid Crystals

Numerous experiments have been done with liquid crystals influenced by QRD. The disorder was produced by silica colloids, aerogel structures or by immersing the liquid crystal in porus materials. A general observation, the QRD smeared the transition and also suppressed the long range nematic and smectic ordering in aerogel mixture [46, 1, 2, 3].

A theoretical approach [12] which modeled the QRD by introducing random fields predicted a destruction of the smectic-A phase by small random field. The same study also predicted the apparition of a "smectic Bragg glass". That last aspect appeared to be discovered by our collaborators in their x-ray experiment [48].

3.3 Calorimetric Results

3.3.1 Preamble

The focus for the phase transition we studied here is on the critical range : $\pm\ 0.005 \times T_C$. In this range the excess specific heat δC_p (obtained by a recipe given below) is proportional to the reduced temperature risen to an under unit value of critical parameter:

$$C_p \propto |t|^{-\alpha} \tag{3.9}$$

The second part of the calorimetry endeavor has a counterpart already published by our collaborators [16] and [48]. The conclusions in their X-rays article are the starting point of this second part that deals with the N-SmA transition. According to that, "smectic 8CB possesses a narrow distribution of layer normal orientations, indicating long range nematic order" [16]. Also, the authors of the above cited paper think that the gel can stabilize the macroscopic nematic alignment along a soft axis. In their second paper they found, unlike in the first paper, that their

data prove a XY Bragg glass behavior [48]. Starting with these, we found changes that can stand for the same kind of conclusions. Our technique gives us complete confidence that the changes we have seen are due to the magnetic field influence. Another aspect of the comparison with the above cited paper is to put the critical coefficients side by side, specifically: α from the calorimetric measurement and $\nu_{\parallel}$, $\nu_{\perp}$ from the x-ray scattering experiment. A side by side comparison between the two sets of parameters will be presented in this chapter. The values found for the critical coefficient α are shown in the Table 3.2.

3.3.2 Overview of ΔC_p versus ΔT_{NA}

Before obtaining the printed form, the raw graph was transformed by subtracting an assumed linear background the same for the lower and upper part of the graph. After that, we had to isolate just the N-SmA transition and we did that by subtracting a fitted wing of the I-N transition from the second order transition range. The formula of the wing was:

$$\Delta C_p = b + l\left\{\frac{T - T_c}{T_c}\right\} + a\left|\frac{T - T_c}{T_c}\right|^{-\alpha} \tag{3.10}$$

In this equation, T_c was chosen at the beginning of the I-N transition temperature from the isotropic side while a, b and l are fitting parameters. The limits of the N-SmA transition were taken at about $\pm 0.005 \times T_c$. The initial trial was twice that big, but the the fittings of the parameters were worse than those presented here.

Figures 3.2 and 3.3 are two different expanded views of the overlap of the six densities of samples in the range of ± 3 K around the transition temperature N-SmA. The starting data of the six densities overlap very well. This is interpretable as the silica presence being manifested only at the very critical limits of the transition. Now, from Fig. 3.2, where the peaks are, one can notice that the nematic side of the graphs have the same shape while the smectic ones start being almost linear after 0.07 g cm^{-3} complementary density. The lower temperature branch represents the formation of the nematic domains inside smectic while in the higher temperature branch is what is left from the smectic domains to be changed into

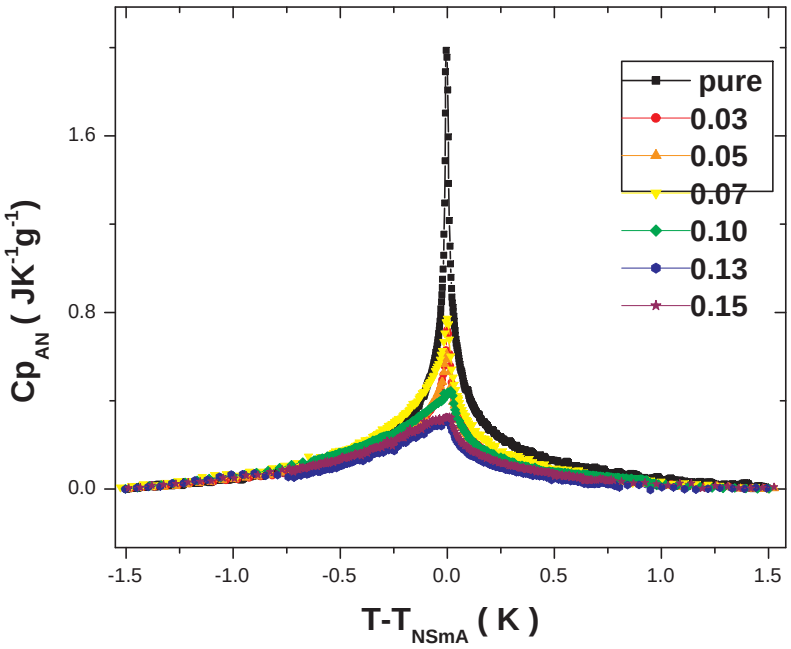

Figure 3.2. The above figure shows, overlapped, the nematic-smectic-A transition with the focus on the very act of transition. The overlap is done for 6 different conjugate densities of silica in liquid crystal (unit in legend is grams of aerosil per cm^3 of liquid crystal).

nematic. In other words, at low temperature there are islands of nematic in a "sea" of smectic and at high temperature the situation is reversed.

Moreover, the peaks start to individualize closer to the very critical region. The height of the peaks is smaller and smaller with the increase in silica density. If one takes into consideration the explanation for the QRD in Chapter 3, this decrease comes naturally because of the increased number of molecules "trapped" in a different phase around the silica beads.

After this first step, we could calculate the enthalpy per unit mass of the transition by integrating the area under the peak. These results are displayed in Table 3.1. In Fig. 3.4, one can see the enthalpy behavior of both random and aligned samples. The enthalpy does not measure any latent heat, as the second order transition does not have one. The general idea is that the trend of enthalpy

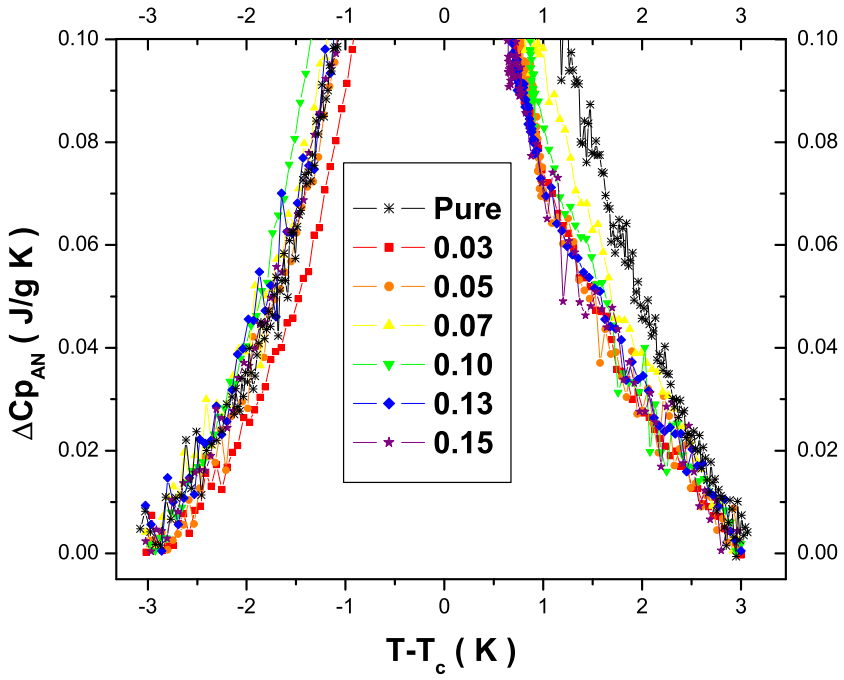

Figure 3.3. The expanded view of the baseline for the N-SmA ΔC_p peaks shown in Fig. 3.2.

with the silica density is complicated to interpret. Nevertheless, one can notice that the enthalpy is increasing as a result of the alignment. If this enthalpy measures how much mobility molecules lost or gained as an effect of the transition, one can tell that indeed the alignment created a sharply anisotropic silica gel as stated by Leheny and coworkers [48]. Now, the gel made the molecules to have higher mobility in nematic phase. This mobility is lost in smectic phase. And that is reflected in the increase of enthalpy as observed. The extra trend gained, with one minima and one maxima, is something that has to be studied more in the future.

3.3.3 Power-law Fitting and Scaling Analysis

The next step is applying the theory of the critical phenomena for the second order transitions. We fitted both sides of the transition peak with the power law given by the Landau theory [8]. Before the fitting, we eliminated the part of the peak

Table 3.1. Transition temperatures and enthalpy of the N-SmA transition for pure, aligned (superscript A), and unaligned (random, superscript R) 8CB+sil samples. Units for T_{NA} are Kelvin and enthalpy J g^{-1}. The value for pure 8CB is independent of alignment.

ρ_S	T^A_{NA}	T^R_{NA}	ΔH^A_{NA}	ΔH^R_{NA}
pure	306.898	306.898	0.731	0.731
.0292	306.293	—	0.506	—
0.0501	305.935	306.092	0.538	0.588
0.0698	305.856	—	0.668	—
0.1011	306.086	—	0.618	—
0.134	306.177	306.327	0.503	0.393
0.1503	306.072	—	0.512	—

where the transition is no longer critical, from just before to just after the peak, at visible inflexion points. A computer program based on the Levenberg-Marquardt algorithm [31] was used to fit the two wings with a formula such as the one below :

$$\Delta C_p = B_c + A^{\pm}|t|^{-\alpha}(1 + D^{\pm}|t|^{\Delta}) \tag{3.11}$$

where:$t = (T - T_c)/T_c$ is the reduced temperature, α is the critical exponent, A is the amplitude of the power law and term $D^{\pm}|t|^{\Delta}$ is the correction to scaling term with D the amplitude of it and Δ is the exponent of the correction to scaling. For the specific heat formula the value $\Delta = 0.504$ is to be found in the theory of the critical exponents [8]. Table 3.2 contains the parameters given by these fittings.

The trend of critical exponent α before and after the alignment is an important part of the analysis. Figure 3.5 contains the 6 aligned samples, two random densities from the same batch with the aligned ones and 4 unaligned densities from Ref. [7]. The trend of the random points is a continuous decrease in the critical parameter up to 0.1 g cm^{-3} in conjugate density followed by a recovery for higher densities. As one can see by inspecting the aligned points, the value of α "stabilizes" in a narrow band between -0.025 and 0.0. Actually, the size of the above mentioned band is the same as the accuracy of determining the critical exponent, so the aligning gives stability to the transition. One might speculate that, after alignment, the critical exponent does not depend on the concentration of silica any more and that stabilizes it to the very value of the 3D-XY model which is -0.013.

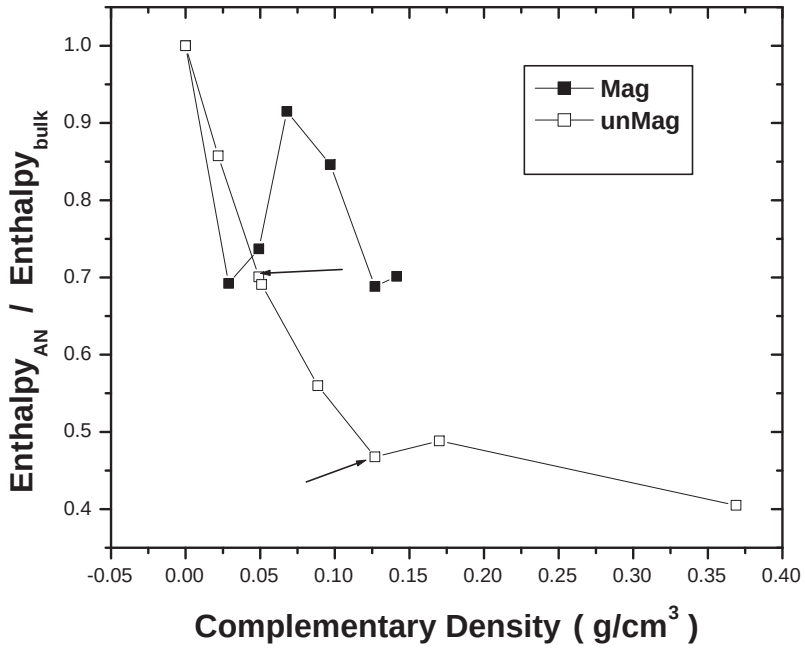

Figure 3.4. The ratio of the N-SmA enthalpy for the 8CB+sil samples versus the bulk 8CB value as a function of ρ_S.

Further more, the stabilization of critical exponent value can be due to the possible fact that before alignment the silica gel might have had dangling branches. When those are in place, the mobility is proportional to the density, whereas when they disappear, the mobility per molecule will be the same regardless of the density.

Another element of the critical behavior indicative of the universality class is the amplitude ratio A^+/A^-. The 3D-XY value is 1.027 (or its inverse 0.9495). The fitting results yield amplitude ratios that are close to the expected 3D-XY value but with much larger uncertainties. Despite this uncertainty, the critical behavior immediately approaches that of the underlying 3D-XY character.

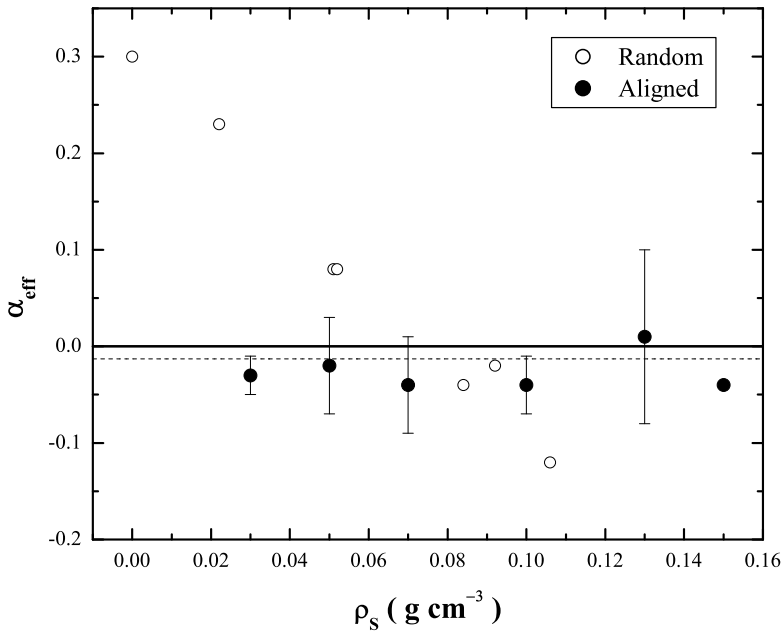

Figure 3.5. The trend of the heat capacity effective power-law exponent α versus reduced density. The filled circles are the aligned samples. The ones from the same batch with the aligned densities are 0.05 and 0.13 g cm^{-3} in conjugate density. The doted line represents the 3D-XY value $\alpha_{XY} = -0.013$.

Another parameter that should be analyzed is the transition temperature. As a prime observation there is a noticeable shift in this parameter. Figure 3.6 contains the N-SmA transition temperatures vs. complementary density. The filled circles are the aligned samples. At a brief inspection one can see that the temperatures are lower in the aligned case. Nevertheless, the trend is the same with the random one.

An explanation of the behavior of the N-SmA transition temperature versus complementary density is the subject of this paragraph. We believe that there is competition between two phenomena. First of all, there is a decrease in the critical point value with the increasing of the conjugate silica density. This is due to the reduction of the mean void size which makes the fluctuations have a better reflection (it is "felt" stronger) in the overall domain (the smectic phase here). In other words, the smaller the domain, the higher probability of a domain or part

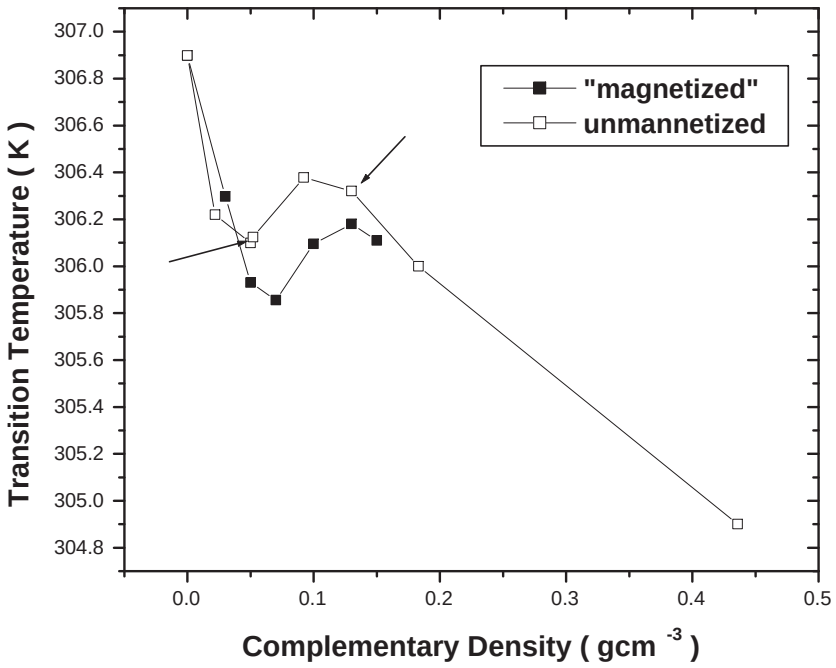

Figure 3.6. Transition temperature of N-SmA transition. The empty squares are the random values taken from [7]. The data pointed with arrows are the random 0.05 and 0.13 g cm^{-3} conjugate silica density. The absolute error is in the range of ± 5 mK.

of it to be switched from a higher order to a lower order phase by a fluctuation in temperature. Some of the domains can get enough energy to boost them up even into the isotropic phase. We regard this last assertion as an explanation of the coupling of the two transitions. This type of behavior is dominant up to conjugate densities of about 0.07 g cm^{-3}, where an increasing back of the transition temperature is dominant. See Figure 3.6. We could interpret that a conformal transformation of better filling the space between the beads causes the mean void to increase right back, leading to an increase in transition temperature up to 0.1 g cm^{-3}, in conjugate density of silica. From then on, the first process is dominant again. The conformal transformation process has a gaussian shape and the quantitative analysis of this is a topic for a future paper.

Also, one can speculate another possible reason to explain the changes measured. The magnetic field might change the long range nematic domains. This can be understood in a way that the "amount of order" of the nematic is less in aligned than in random so automatically the transition happens at lower temperatures. This stands for the I-N transition as well. Because the two transitions are very close (7 K), hence coupled, the N-SmA and I-N transitions influence reciprocally. The size of the change in the second-order transition is ~ 3 times smaller than for the first-order transition.

3.3.4 X-ray and Calorimetry Critical Behavior Comparison

A scaling and hyper-scaling analysis is something to be done to prove the case in favor of the modern theories about second order transitions. Studying the critical exponents theory [8], the scaling laws reads:

$$\xi_{\parallel} = \xi_o t^{-\nu_{\parallel}} \tag{3.12}$$

$$\xi_{\perp} = \xi_o t^{-\nu_{\perp}} \tag{3.13}$$

$$\delta K_2 \propto \xi_{\perp}^2/\xi_{\parallel} \tag{3.14}$$

$$\delta K_3 \propto \xi_{\parallel} \tag{3.15}$$

$$B \propto \xi_{\parallel}/\xi_{\perp}^2 \tag{3.16}$$

$$D \propto \xi_{\parallel}^{-1} \tag{3.17}$$

$$2 - \alpha = \nu_{\parallel} + 2\nu_{\perp} \tag{3.18}$$

$$\gamma = (2 - \eta_{\perp})\nu_{\perp} \tag{3.19}$$

Note that the α from Table 3.2 was inserted in Eq. (3.18) and the values of $\nu_{\perp}$ and $\nu_{\parallel}$ were taken from an article of our collaborators [48]. We did the simple calculations starting from densities in the above cited paper and interpolating or, by the case, extrapolating the value for α. The results can be read in Table 3.3. As one can see, the correspondence between the two sets of data is very good.

Table 3.2. The values in next table are the critical parameters of N-SmA transition.

ρ_s	α	T_c	B_c	A^+	A^-/A^+	D^+	D^-/D^+
Aligned							
0.0	0.30±0.01	306.972	-0.421	0.076	1.049	5.171	0.723
0.03	-0.03±0.02	306.293	6.552	-7.672	1.031	-0.168	3.859
0.05	-0.02±0.04	305.931	8.430	-9.309	1.024	-0.055	7.040
0.07	-0.04±0.05	305.858	4.316	-5.299	1.051	-0.137	6.524
0.10	-0.04±0.05	306.143	2.834	-3.268	1.081	0.530	-1.079
0.13	0.01±0.05	306.175	-7.973	7.748	0.979	-0.191	-0.428
0.15	-0.04±0.07	306.090	2.884	-3.482	1.045	-0.006	79.881
Random							
0.05	0.15±0.05	305.926	-1.410	0.990	0.922	0.007	150.88
0.13	0.06±0.05	306.270	-1.292	0.980	0.940	-0.074	-9.29

Table 3.3. The values in the table beneath were obtained from Leheny et.al. [48]. The calculation reports the range of values propagating errors.

ρ_S	$2-\alpha$	$\nu_\parallel - 2\nu_\perp$
pure	1.70	1.69
0.027	2.01 - 2.05	2.07 - 2.18
0.042	1.98 - 2.08	1.97 - 2.11
0.071	1.91 - 2.01	2.01 - 2.13
0.100	2.01 - 2.07	1.95 - 2.11

Taking into account that the experiments were done two years apart with different samples obtained in different places, one can tell that it is a very good proof for efficacy of the critical exponents theory.

As for the meaning that the annealing makes the critical coefficient α almost constant, there are other ways to speculate. Looking at Eq. (3.17) and with the contribution of Eq. (3.12) one can extract $D \propto \xi_o^{-1} t^{\nu_\parallel}$. From the already cited Eq. (3.18) if α becomes lower, $\nu_\parallel$ becomes lower so, for common values of t between $10^{-5} - 10^{-2}$, D becomes smaller. On the other hand, D is regarded as the energy needed to tilt the director away from the layer normal [8]. The conclusion is that the alignment makes the mixture more rigid for some and also less dependent on the silica density. In other words, a significant increase in silica density does not

contribute as much as the small density did. The last statement is similar to the one already mentioned at the beginning of the chapter that "the alignment can stabilize the macroscopic nematic alignment along a "soft axis".

3.4 Discussion and Conclusions for the *N*-Sm*A* Transition

This part of the experiment, analyzing the nematic to smectic-A transition of a set of samples that were previously "aligned" in a magnetic field, had proved its purpose. We measured the well known macroscopic parameters and they changed in a way that it made sense for, in part for the theories in hand and in part for some new logical consequences.

With respect to the random, unaligned samples, the N-SmA transition temperature is diminishing for all the samples. The critical exponent stabilizes immediately, beginning at the lowest ρ_S sample studied, to a near 3D-XY value. Although, the amplitude ratio is consistent, the uncertainties are much larger.

The comparison between the present calorimetry data and the x-ray counterpart [48] reveal a consistent behavior with that expected from scaling. Although orientationally aligned, the random pinning of the SmA layers still exist and so the random-field like model should still hold.

Chapter 4

DIELECTRIC SPECTROSCOPY

4.1 Overview of Dielectric Spectroscopy

The technique of dielectric spectroscopy is an old, though very accurate technique for measuring the dielectric constant (electric permittivity) of various materials and substances. One reason we are still using it today is to do research on materials never before investigated. Another reason is because accuracy has been improved dramatically with the appearance of the lock-in amplifier. Also, the use of high-speed, extensive memory computers to completely automatize the experiment has been essential. This last aspect allows the obtaining of much higher accuracy in our experiments because the computer can run the experiment without interruption for days or months and also the computer never fails one reading.

Another kind of measurement involves a relaxation process. This consists in spanning the frequency to discover the relaxation time of different processes. More specifically, by applying a sinusoidal signal of various increasing frequencies, one might find values where the molecules can no longer follow the input frequency. That last aspect is a qualitative identification of a relaxation process hence a rotational mode of the molecules. To quantitatively find the frequencies one should use the Debye formula:

$$\overline{\epsilon} = \epsilon_\infty + \frac{\Delta\epsilon}{1 + i\omega t} \tag{4.1}$$

with $\Delta\epsilon = \epsilon_S - \epsilon_\infty$, ϵ_S permittivity under DC current or very low frequency, ϵ_∞ permittivity at very high frequency. The quantity $\overline{\epsilon} = \epsilon^{'} + i\epsilon^{''}$ is a complex value for

the dielectric constant which puts on the same foot the alignment of the sample by the real $\epsilon^{'}$ and the loss by the imaginary one $\epsilon^{''}$. For multiple relaxation processes the Havriliak-Negami formula should be used. Another procedure for extracting new facts from the experiment is to use Arrhenius formula:

$$\tau = \tau_o \, e^{\Delta E/(k_B T)} \tag{4.2}$$

with τ the relaxation time, ΔE the activation energy, k_B the Boltzmann constant, and T the absolute temperature. The value of activation energy can help speculate about the energy attributable to a molecular rotational mode. Keep in mind that the above formula is severely trespassed for liquids with higher viscosity which most of the liquid crystals are.

4.1.1 Proxy for Nematic Order

What makes dielectric constants to be so valuable? The more aligned the molecules are, the bigger the capacitance is. By excellence, liquid crystals are all about the order. There polar molecules generate a electric dipole. These dipoles align in the nematic state which leads to an increase of the capacitance which is due to a change in dielectric constant. So, there is a direct link between the permittivity and the order parameter of the liquid crystal. Nevertheless, the connection is very complicated and it has not yet rigorously discovered.

The dielectric constant being an easily measurable quantity, theoreticians tried to connect it with the parameter that intimately governs the liquid crystals. Among the theories currently used by the scientific community, the one of interest here belong to Maier and Meier (M-M) [50, 53, 56]. Starting from the Osanger theory of liquid crystals, M-M developed the formula:

$$\Delta\epsilon = \epsilon_{\parallel} - \epsilon_{\perp} = \frac{NhF}{\epsilon_o}[(\alpha_l - \alpha_t) - \frac{F\mu^2}{2kT}(1 - 3\cos^2\phi)]S \tag{4.3}$$

where α_l and α_t are the parallel and perpendicular polarization, N is density, ϕ is the angle between the dipole and the long molecular axis; for 8CB that could be zero , $h = \frac{3\overline{\epsilon}}{2\overline{\epsilon}+1}$, $F = (1 - \frac{\overline{\epsilon}-2N\overline{\alpha}}{2\overline{\alpha}+3\epsilon_o})^{-1}$ with $\overline{\epsilon} = (\epsilon_{\parallel} + 2\epsilon_{\perp})/3$ and $\overline{\alpha} = (\alpha_{\parallel} + 2\alpha_{\perp})/3$.

If one compares the above formula with the temperature dependency of the

order parameter from the Landau-deGennes model for the nematic phase:

$$S = S_o + S_1(\frac{T_C - T}{T_C})^{\beta}, \tag{4.4}$$

one should be able to extract the critical coefficient β and to compare it with the one from different other models. Landau-deGennes theory [8] predicts for bulk liquid crystal value for β of 0.5.

4.1.2 Previous Experimental Results

The formulas that end the previous paragraph were cross cited from the work of J. Thoen [50] where he reported the value that had been mentioned for the critical parameter β but also the parallel and perpendicular static dielectric constant for 8CB. The data they got for 8CB, published in the above cited paper can be seen in Fig. 4.11 with both parallel and perpendicular values for the permittivity. There are many later contributions in the research of liquid crystal with dielectric spectroscopy but we will mention only the ones where QRD has a role.

J. Thoen et.al. had studied [51] 7CB and 8CB liquid crystals with dielectric spectroscopy to find three different relaxation frequencies 34.3, 225 and 600 MHz at 44.4 ^{o}C, which is in isotropic. They found only one frequency in the parallel alignment and they claim that the frequency is temperature independent for a very significant range of temperatures.

In 1998, Sinha and Aliev [55] did broad band dielectric spectroscopy on 5CB and 8CB confined in random interconnected silica glass pores. They used 0.01 and 0.1 nm size porus which correspond to silica beads dispersion of 0.5 and 0.07 g cm^{-3}. For 8CB, they found a frequency around 5 MHz attributed to the rotation of the molecule around the short axis and also one of 70 MHz attributed to a librational (hampered tumbling mode). The first one was an Arrhenius relaxation type. A very trustfully temperature dependency for 0.1 nm pores shows a sharp decrease of the frequency of the rotation around the short axis with temperature decreasing. In confined liquid crystal the processes are not frozen even at temperatures 20 K below the crystallization point. Another novelty found was a relaxation which is not seen in bulk and which they attributed it to the hampered rotation of molecules next to the silica wall. By this they made an estimate of the size of the interaction

energy between liquid crystal molecules and silica wall being ~ 0.05 J m^{-2}. A very counterintuitive observation is that the highest frequency mode, due to tumbling, is vanishing in the isotropic phase where there is no defined director.

In 2001, Hourri et.al. [52] performed broadband dielectric measurement on 5 silica density dispersed in 7CB. This liquid crystal does not have a smectic phase. For ones the trend of the transition temperature versus the silica density is the same for 8CB meaning that the same mechanism is behind both. Here too a small frequency process not observable in bulk is noticed and attributed to a hindered rotation of the molecules in the layer next to the silica beads.

A new experimental technique was used by Aliev et.al. [56] where a 0.2 nm diameter cylindrical pores Anopore membrane was treated with lecithin. The authors claim that they have created a radial alignment of the molecules in pores and thus a perpendicular alignment to the electric field applied. Even thou we doubt that claim, they might of changed the forces of interaction with the wall. A qualitative discussion, was done using dielectric strength of the M-M theory given by Eq. (4.3) mentioned above. According to that, the orientational order parameter decreases while the temperature approaches the clearing point.

In 2005, Sinha et.al. [54] studied 5CB in treated and untreated Anopore membranes and in 3 densities of samples with dispersed silica. For the latter part they treated the electrodes clamming to have the molecules homeotropically aligned for a good comparison with the Anopore case. Their conclusion was that relaxation time decreases with an increase in silica concentration. Another important conclusion was obtained with dielectric strength analysis, which ultimately measures orientational order parameter. That was a decrease of the order parameter with an increase of silica concentration.

The same group has studied 10CB in treated and untreated Anopore and in Vycor porus glass. The 10CB does not have a nematic phase and exhibit an isotropic-smectic transition at 50.2 ^{o}C. The author now made a rule that there are 3 modes. A fast rotation around the short axis, an even faster librational mode due to tumbling and a slow process due to surface interaction. In Vycor one can see similar processes, even a kind of surface interaction. The systems in Vycor glass can be supercooled at least 185 K below the crystallization temperature and which was the lowest they had to test. In that they saw a glass like transition. The

group also studied 0.08 and 0.31 g cm^{-3} dispersed hydrophillic silica. The main relaxation process slows down with the temperature and has a jump at the I-SmA phase transition. The two mentioned densities have almost the same values. For the surface interaction mode there is close to no temperature dependency for either density.

Rivera and Aliev [57] investigated 8CB in Anopore with 3 different filling percentage: 100, 15, and 8 %. There was a increase in relaxation time of the low frequency process (due to interaction with the walls) with the diminishing filling percentage. That was attributed to an increase in viscosity in thinner layers. The high frequency rotational mode in isotropic becomes a librational mode in nematic and can be observed even in parallel alignment attributed only to the fluctuations of the dipole moment.

Finally, there is an exotic experiment by Aliev et.al. [58] with 5CB in nanopores only $2-3$ nm in diameter. As a consequence, one pore can only accommodate one molecule, considered a 1-D system. They found no nematic phase and also the possibility of supercool it indefinitely. That is understandable because the molecules were unable to interact with each other.

4.2 Experimental Technique

4.2.1 Theory for Capacitive Measurements

As a principle, the dielectric spectrometer is a capacitor (preferably a parallel plates one) with the dielectric material inserted in between the two plates. The fringe effects are completely negligible because the distance between the plates is very small and also because this distance is two orders of magnitude smaller than the diameter of the plates. By applying an AC current, one can measure the capacitance and obtain the electric relative permittivity (for simplicity, from now on we will call it just permittivity). Ultimately one can link permittivity with the order parameter of the substance.

The formulas governing the plane capacitor are:

$$C = C_{inv} + \frac{\epsilon_o S_{air}}{d} + \frac{\epsilon_o \epsilon_r S_{sample}}{d} \tag{4.5}$$

$$C_{empty} = C_{inv} + \frac{\epsilon_o(S_{air} + S_{sample})}{d} \tag{4.6}$$

with C_{inv} is the capacitance of the environment, S_{air} is the area not filled with the sample, d is the distance between the plates, $\epsilon_o = 8.8542 \times 10^{-12}$ F m^{-1} is the absolute permittivity of the free space - almost equal to the air, ϵ_r is the relative permittivity, and C_{empty} is the capacitance of the empty capacitor. This relative permittivity is also called the real one as opposed to an imaginary one derived from electrical resistance as will be seen further more. Thus, the final formula for real dielectric constant is:

$$\epsilon_r \equiv \epsilon^{'} = 1 + \frac{d}{\epsilon_o S_{sample}}(C - C_{empty}) \tag{4.7}$$

Now, because the measurements are taking place in an AC current, there is also a resistance of the sample involved due to the ions migration. In a widely spread approach, one can consider permittivity to be a real one and permittivity derived as follows to be an imaginary one. If one considers resistance R and capacitive reactance $X_C \longleftrightarrow R$ (being alike quantities) than from $R = X_C = \frac{1}{\omega C}$ (where the equal sign is informal meaning just that the two are alike quantities) and $C = \frac{\epsilon_o \epsilon^{''} S}{d}$ it results:

$$\epsilon^{''} = \frac{1}{\omega(\frac{\epsilon_o S}{d})R} \tag{4.8}$$

so one can define a complex relative permittivity:

$$\epsilon^* = \epsilon^{'} + i\epsilon^{''}. \tag{4.9}$$

From a phasor representation of an AC circuit, one can extract the resistance of the sample and imaginary permittivity. The geometric relations are

$$tan\varphi = \frac{I_C}{I_R} \;\Rightarrow\; tan\varphi = \frac{1}{\omega CR} \;\Rightarrow\; R = \frac{1}{\omega C tan\varphi} \tag{4.10}$$

where C is the capacitance, $\omega = 2\pi\nu$, ν is the frequency, and φ is the angular phase difference between the current phase an the one measured at the beginning with the bridge balanced. Of course, the imaginary permittivity is given by:

$$\epsilon^{''} = \epsilon^{'} \tan\varphi \tag{4.11}$$

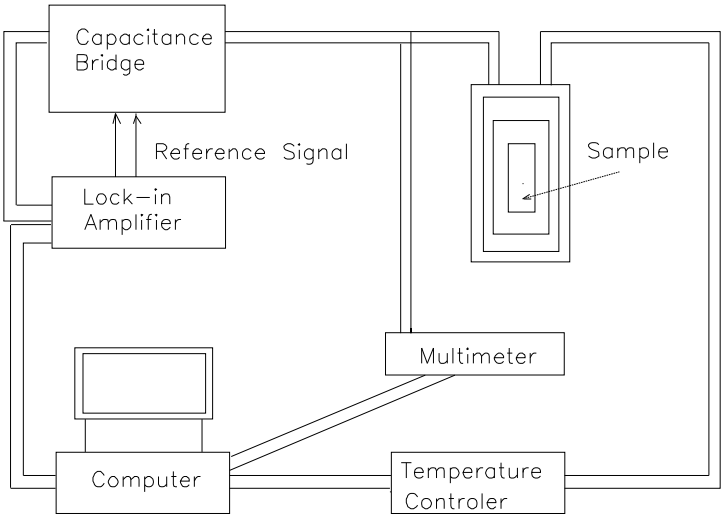

Figure 4.1. Electric circuit diagram for the ac-capacitive bridge dielectric spectrometer.

4.2.2 Experimental Setup and Characteristics

By measuring the capacitance directly, one can not surpass a certain precision level due to the omnipresent noise. If a capacitance bridge (also known as a Wien or Wheatstone bridge) is used, as we have done in our experiments, then the precision can go up to 10^{-4} pF. The electrical circuit of the experimental set-up can be seen in Fig. 4.1. The manual capacitance bridge type-1610A made by General Radio was used. The lock-in amplifier was a Stanford Research Systems model-840, the multimeter was a Keithley model-2000 of 1 pA precision, and the temperature was controlled with a Lake Shore model-340 dedicated device.

The lock-in amplifier was also used to apply the reference signal in one arm of the capacitance bridge but only up to 5 V which was the upper limit of that particular one. Later, that was compensated by introducing a powerful amplifier which could output a voltage of up to 50 V, but for the capacitor in hand, that meant almost the limit of electric breaking of the air surrounding the active substance. The frequency of the input voltage was up to 100 kHz but the one actually used was 10 kHz. That limited our experiments from covering the typical main relaxation processes. The lock-in amplifier was also used as a detector in the other arm of the bridge, also being capable of measuring the phase shift of the signal. The latter, intimately meant to measure the very small conductivity of the dielectrics.

This is important in phase transitions because the conductivity can bring one more parameter for the understanding of the process at hand.

The most used way of the set-up was to ramp the temperature up and down and to measure the capacitance while the sample was in between the capacitor's plates.

In Fig. 4.2, one can see the experimental setup which basically consists of two small cylinders, two pucks , with very flat surfaces facing each other. A dielectric ring keeps them apart at a very precise distance (in this experiment was 250 μm). The dielectric under study had to be inserted in the gap between the plates. The pucks were held apart with a dielectric ring. The upper puck has a hole drilled to accommodate a 100 Ω platinum thermometer which measures the temperature in the very vicinity of the of the sample, thus assuring a very high confidence in temperature value. The two pucks are held together tightly by discs at one end of each; the discs are bolted together. The ensemble described hangs from the cap of a copper cylinder. The latter has a whole drilled in the side meat where a diode thermometer was inserted. All around the copper cylinder there is a foil heater which provides the necessary heat, controlled by the thermometer just described. The copper cylinder is fit into a bigger aluminum cylinder which provides a better insulation from the environment thus a higher stability of the temperature. Inside the copper cylinder there is a desiccant which absorbs the humidity. The electric wiring is passed through the caps with dedicated connectors.

The capacitance bridge being manual, one cannot use it fully in the balanced position. Thus, it has been used by balancing it at a temperature where we knew that from then on the capacitance would only increase or only decrease, taking it away from the equilibrium position. Nevertheless, the capacitance is proportional with the amplitude measured by the lock-in amplifier. The multimeter was there only for the part of the experiment where an increasing voltage was applied to the sample.

4.2.3 Sample Preparation and Loading

The samples for the current experiment were mixtures of silica and 8CB liquid crystal from the same batch (same vials) like the ones used in the AC experiment.

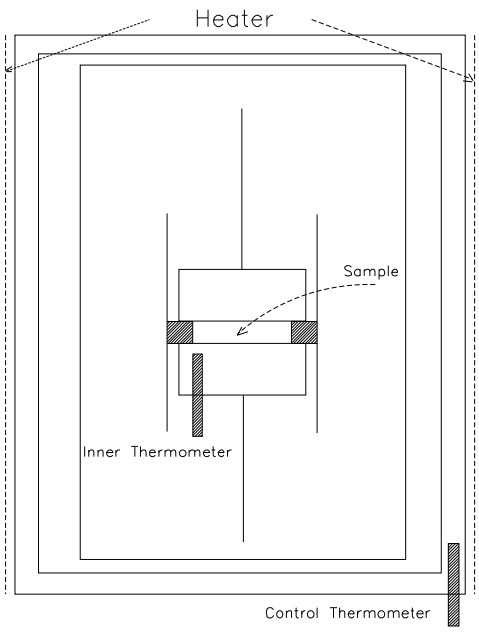

Figure 4.2. The scheme of the sample holder. The heater is a sheet surrounding the outer cylinder.

To load the sample, the desired amount of mixture should be chosen as to not overshoot the space delimited by the two parallel plates and the separation data ring. Then, this quantity is deposited on the lower puck and placed under vacuum (again $\sim 10^{-3}$ Torr) at $\sim 39\ ^{o}$C for about two hours. The procedure is used to get rid of the water and the temperature used for that is a cautionary value because a higher one would led to boiling and spiling the mixture all over the place and loosing it. Once this is done, the lower puck is put together with the upper one and bolted. Then the assemble is placed in the aforementioned copper cylinder mentioned before. At the bottom of that cylinder a granular desiccant is placed to absorb the water vapors which otherwise will reach the sample. All the connectors are plugged into the cap of the copper cylinder and this one is placed inside the bigger aluminum cylinder. The aluminum cylinder has an insulating fabric wrapped around its inner surface. On the bottom of the aluminum cylinder, a wooden ring assures a proper exit of the wiring of the control thermometer, which allows for the wires to be placed in the groove of that ring.

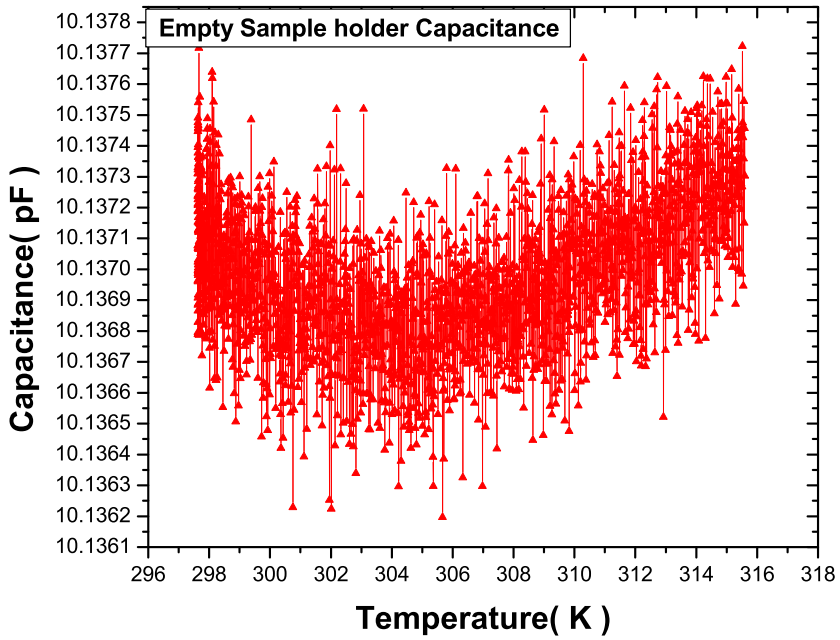

Figure 4.3. Empty sample holder capacitance as a function of temperature over the same range as the 8CB liquid crystal undergoes two phase transitions. The linearity is quite good with a long-term stability of approximately $\pm 5 \times 10^{-4}$ pF.

4.2.4 Experimental Procedures

Various computer programs, written in C++, have been used to run the experiments. This allowed the collection of thousands of data points in a matter of hours, while the temperature or the amplitude was varied, maintaining the other parameters constant. The experiments performed with the dielectric spectrometer were to reveal aspects that other techniques could not. A proof of the performances our set-up could attain is the Fig. 4.3 representing the capacitance of the empty capacitor while the temperature spanned the main range used in the experiment: $\sim 300-320$ K. The data were obtained without mediation and precision was better than 10^{-4} pF. One can calculate, with very high accuracy, the dilation of the brass material the pucks are made of using our set-up.

Experimental Procedure Part 1.

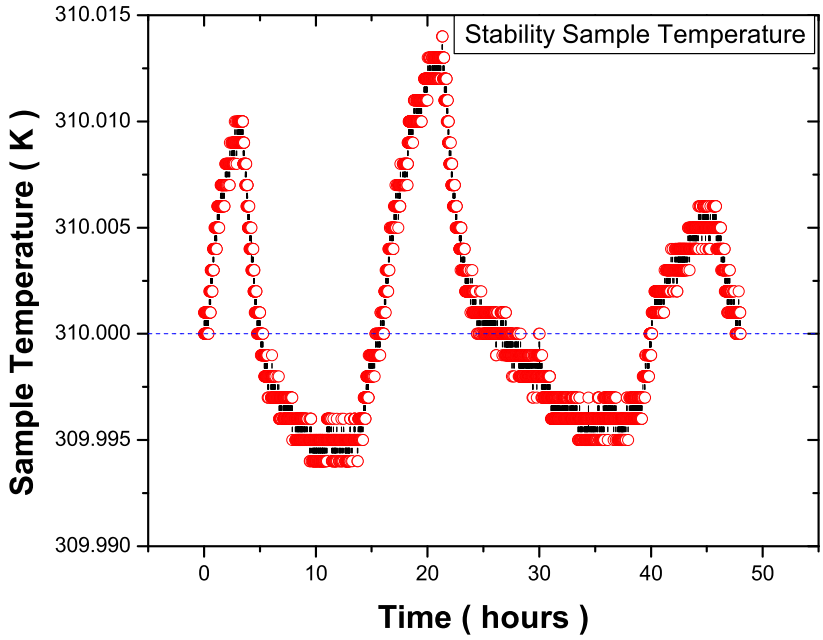

Figure 4.4. The stability of the temperature of the first experimental procedure for two days. This indicates an absolute thermal stability of ±0.015 K.

In this procedure, the samples were kept at a constant temperature of $\sim$ 310 K. That was achieved by fixing a control temperature at 311.5 K but, due to an internal lag, had the approximate value mentioned before. Nevertheless, the precision of maintaining a specific value for temperature for the duration of the experiment was ±10 mK. This aspect is revealed in Fig. 4.4. At that temperature, the sample was subject to application of AC voltage in portions of two minutes with increase in amplitude from zero to $\sim$ 45 V. This was the equivalent to a $\sim$ 180 kV/m electric field. After each of those "shocks", the capacitance was measured. The final outcome of the experiment was a dependency established between the applied electric field and the new capacitance measured right after that.

Experimental Procedure Part 2.

For the second procedure the mixtures were subjected to three cooling scans. The first was done right after the sample was loaded and heated up to its isotropic state. The second scan was done after the application of a procedure that tried to mimic the one performed with the magnetic field as described in the first chapters. This time we applied a field of 80 kV/m (produced with 20 V) for 48 hours while the temperature was ramped up and down, over one hundred times, in between ~ 310 and ~ 318 K. In fact, an intermediate scan was done with no field applied. Thus, all three cooling scans were done from $\sim$ 319 K down to $\sim$ 300 K. In this experiment the goal was to see changes of the transition temperature and to interpret them. Another goal was to see the possible changes in permittivity which had to ultimately be related to the order parameter.

4.3 Results

4.3.1 Annealing Electric-Field Study

After every applied pulse mentioned above, the capacitance was measured. We expected to initially see a plateau where the capacitance was unchanged after every "shock" applied, followed by a constant increase in capacitance after surpassing a certain value of the voltage. In the end, we would expect to see a new plateau with the impossibility of being surpassed by any applied voltage. The difference between the electric field giving the higher plateau and that giving the lower one should be a measure of the strength of the interaction between the liquid crystal molecules and the silica beads. Furthermore, the the difference in capacitance would also have to be a measure of that interaction.

The above experimental procedure was meant to reveal a possible alignment of the liquid crystal molecules around the silica beads. The idea was that liquid crystal molecules arrange locally around the silica beads as in Fig. 4.5. Farther away from the beads, the liquid crystal molecules become arranged according to the nematic director or the smectic layering, depending on the phase they are in. By applying an electric field of a specific intensity, at some point this will be stronger than the force which makes the molecules and the silica beads to attract each other. Thus, the molecules will align better with the electric field direction,

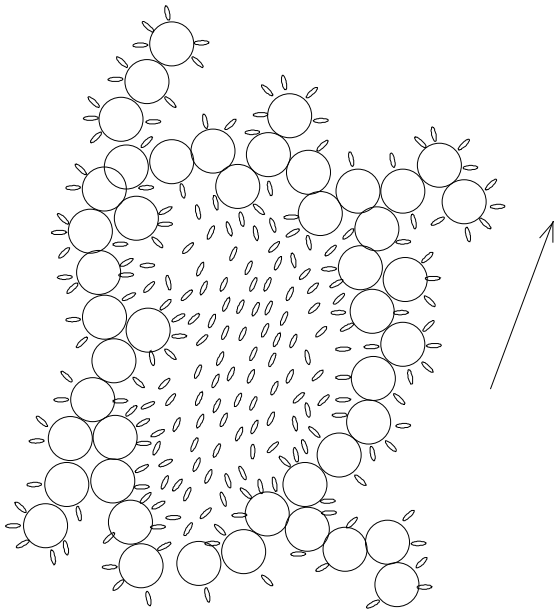

Figure 4.5. The figure depicts the colloidal mixture between the silica beads and the rod-like molecules (similar to 8CB). The arrow exaggerates the preferred direction of the molecule in the space away from the silica beads. That is supposed to be the nematic director.

even locally. The situation is depicted in Fig. 4.6. The best way to picture what is happening is to imagine a colic in ones human hair. The same way liquid crystal molecules should align, leaving a "colic" around the equator of the beads after the applying of the electric field . This is professor Iannacchione's idea and the following calculations seems to consider it a possible explanation.

So, the liquid crystal molecules which are interacting directly with the beads should change the preferred average position from a radial one to one where they point more in one direction. This would be due to the increase of the alignment and, as a consequence, of permittivity.

The actual results of the experiment were not very clear in confirming the plateau theory. A different approach is to calculate the change in energy in two ways. The first is to consider the change in capacitance with the elementary formula:

$$\Delta W_1 = \frac{\Delta C\ U^2}{2} \tag{4.12}$$

The second is to calculate the energy as a dipolar interaction multiplied by the

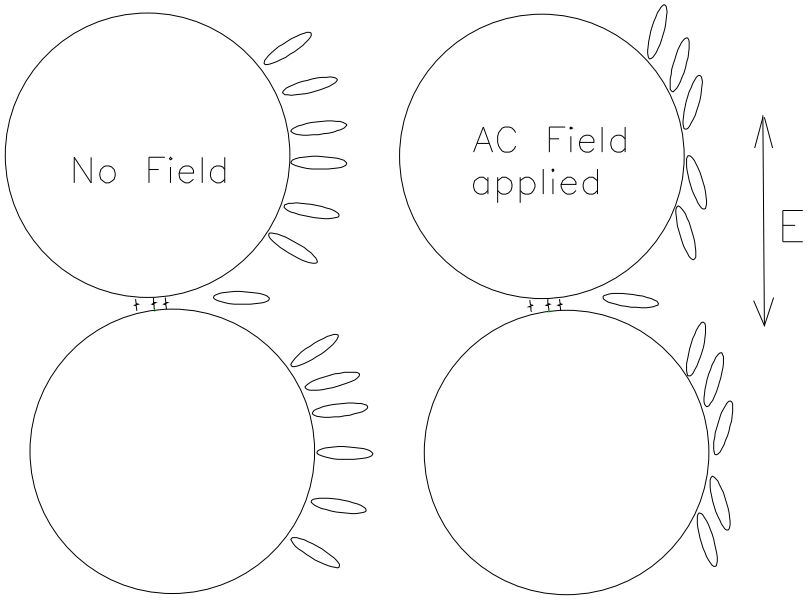

Figure 4.6. The picture depicts the hypothetical influence that the AC-field would have towards the liquid crystal molecules that are initially radial around the silica beads and after applying the electric field arrange themselves as seen in the right part of the picture.

assumed number of molecules considered to be involved in the process:

$$\Delta W_2 = -N\overrightarrow{p}\cdot\overrightarrow{E}. \tag{4.13}$$

If one calculates the values for the two energies, they should consider some generic values for the quantities involved which are: the dipole moment for 8CB liquid crystal of ~ 5 D (the international unit for the electric dipole, $1 Debye = 3.33564 \times 10^{-30}$ C m); the electric field $E = U/d$ with $U = 0.2$ V the voltage used to measure the capacitance and $d = 250$ μm the distance between the plates; we chose $\sim 35^o$ as being an assumed possible new average angular position of the molecules and not taking into account any distribution of that angle. N is the number of molecules that underwent the process described and its calculation is not a trivial task. For the first energy, a generic value of the change in capacitance $\Delta C \simeq 20$ pF is

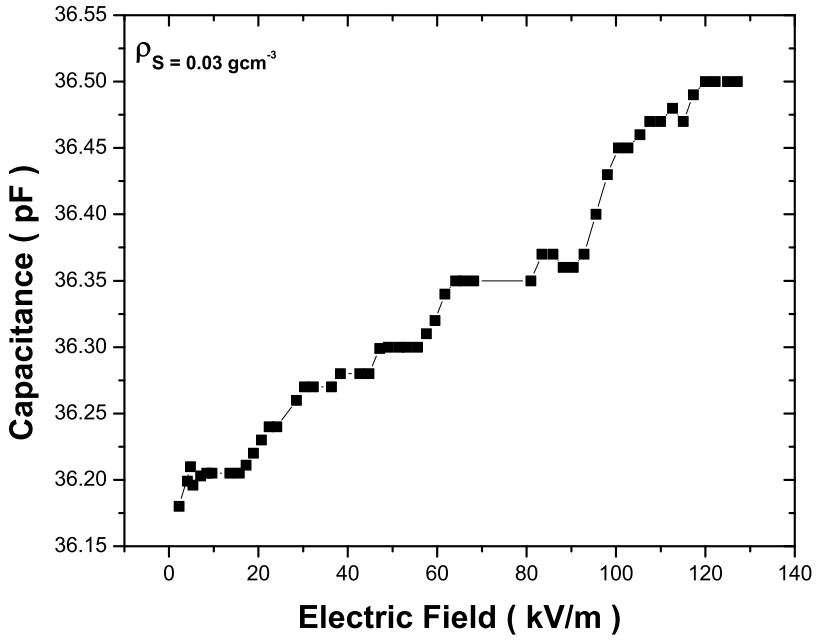

Figure 4.7. Capacitance versus applied field for $\rho_S = 0.03$ g cm^{-3}.

observed from Figures 4.7, 4.8, 4.9, and 4.10. The results of that calculation are:

$$\Delta W_1 \simeq 4 \times 10^{-15}\ J \qquad \Delta W_2 \simeq P \times 8.5 \times 10^{-15}\ J \tag{4.14}$$

where P is the percentage from all liquid crystal molecules that are in the position to undergo the change in relative position around the silica beads. The mass used was a generic value of 20 mg.

As one can see, the two values are fairly close especially if the percentage of molecules involved would be $\sim 10\%$ range. If the range we are looking for is $\sim 1\%$, some other mechanism should be accounted for the increase in capacitance as will be seen in the last paragraph.

We used 7 different densities but only the lower ones gave relevant data and are shown in Figures 4.7, 4.8, 4.9, and 4.10. For the higher densities there was now change in capacitance recorded and the reasons for that are not clearly understood by any of the models discussed previously. We speculate later on other possible

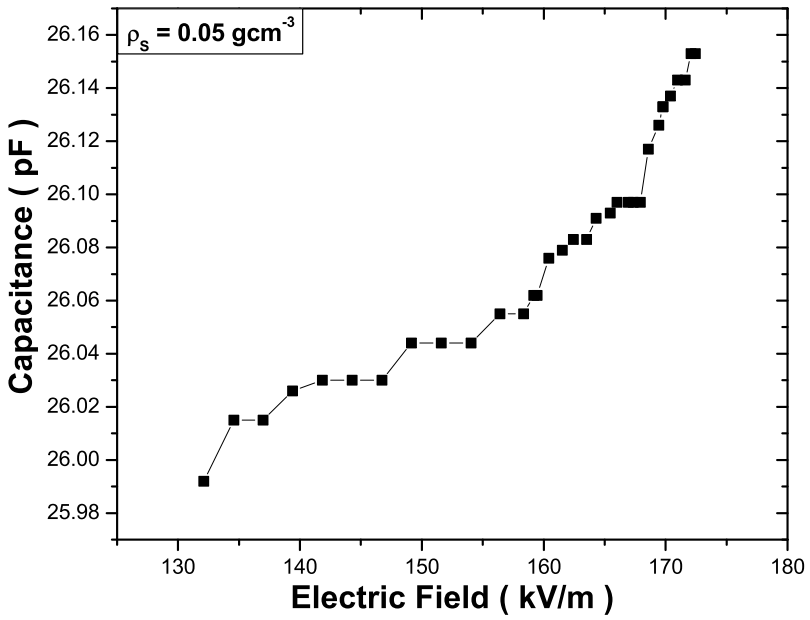

Figure 4.8. Capacitance versus applied field for $\rho_S = 0.05$ g cm^{-3}.

mechanisms in play.

4.3.2 Temperature and Electric-Field Cycling Study

The results for pure 8CB could be verified with our main reference [50], as one can see in Fig. 4.11, representing permittivity versus temperature, in the domain range where this liquid crystal undergoes two transitions. The results of our pure 8CB in the form of a quantity proportional to the order parameter is in Fig. 4.12. The difference between the results is that the first one had a bigger range covered and also the possibility to obtain molecules aligned parallel and perpendicular. Our data could much better map the transition - there are around 5000 points per any of the graphs - a quality that has not yet been exploited.

The results obtained from reading the plots of the resistance or the imaginary permittivity are not relevant. In Fig. 4.13 for the resistance of a generic density and for the imaginary permittivity both taken versus temperature, do not give any insight of the behavior of the mix 8CB liquid crystal and hydrophilic silica beads.

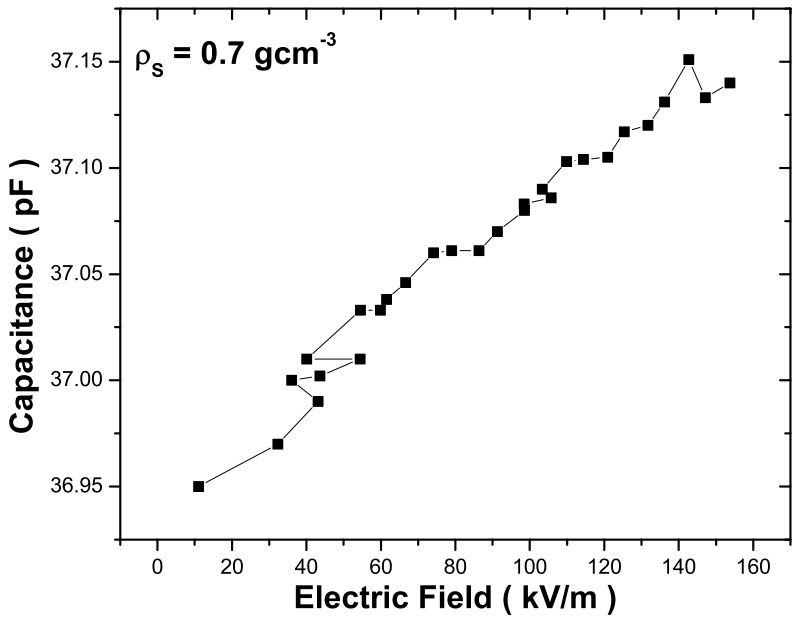

Figure 4.9. Capacitance versus applied field for $\rho_S = 0.07$ g cm^{-3}.

The main approach in this section is to consider a simplified formula from Maier and Meier's theory (see Ref. [56]). According to that, the dielectric strength $\Delta\epsilon$ has the following connection with the order parameter:

$$\Delta\epsilon \simeq \frac{\mu^2(1-S)}{k_B T} \tag{4.15}$$

where $\Delta\epsilon = \epsilon_S - \epsilon_\infty$, μ is the dipole moment, and k_B is the Boltzmann constant.

With our technique we did not get ϵ_∞ and ϵ_S. The first one represents the permittivity at very high frequency where all the rotational and vibrational modes could not follow the input signal frequency and the value will be given only by polarization of the atoms and molecules as wholes. The second value, the static one, has all rotational and vibrational modes unperturbed, the translation not being "seen". Thus, the difference between the two is a measure of the average angular position of the dipolar molecules with the polarization being "subtracted". However, this is just what the order parameter represents.

In our case, we subtract out the current value from the one at the isotropic to

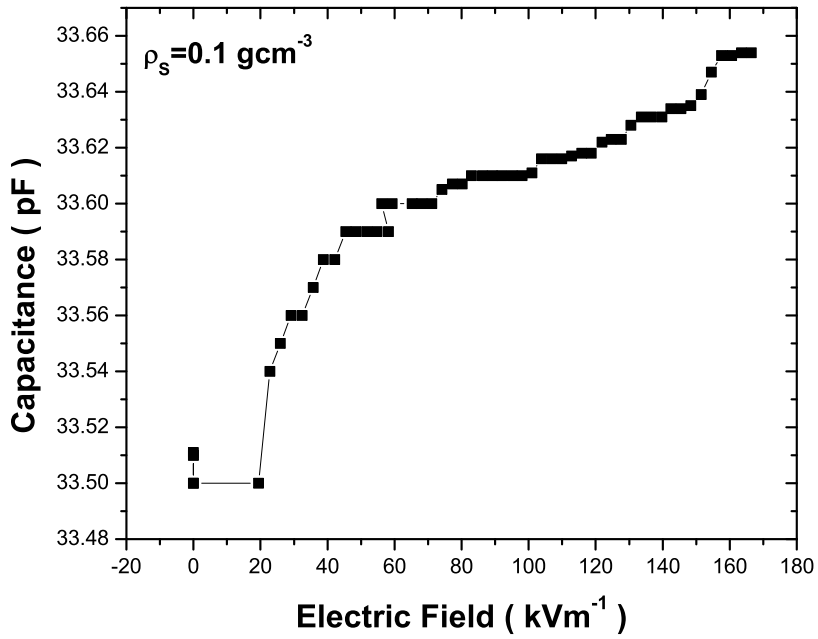

Figure 4.10. Capacitance versus applied field for $\rho_S = 0.10$ g cm^{-3}.

nematic phase transition. This measures the changes in order parameter caused by the transition so the value reflects major qualitative and quantitative - still, unscaled - changes due to the transition. In other words, it might not follow some modes that are manifest in both phases, but it was a good measure for the mode that changes at the transition.

If one extracts S from Eq. (4.15), the temperature dependence is given by

$$S = 1 - K\ \Delta\epsilon(T)\ T \tag{4.16}$$

with K just a constant of proportionality. The picture is not complete because one needs a reference point to compare the different densities. The most natural mode is to consider the value for S as being zero at the transition which leads to:

$$S = 1 - \frac{\Delta\epsilon(T)}{\Delta\epsilon(T_{NI})}\ \frac{T}{T_{NI}} \tag{4.17}$$

The above formula follows two figures that group together 6 different densities and

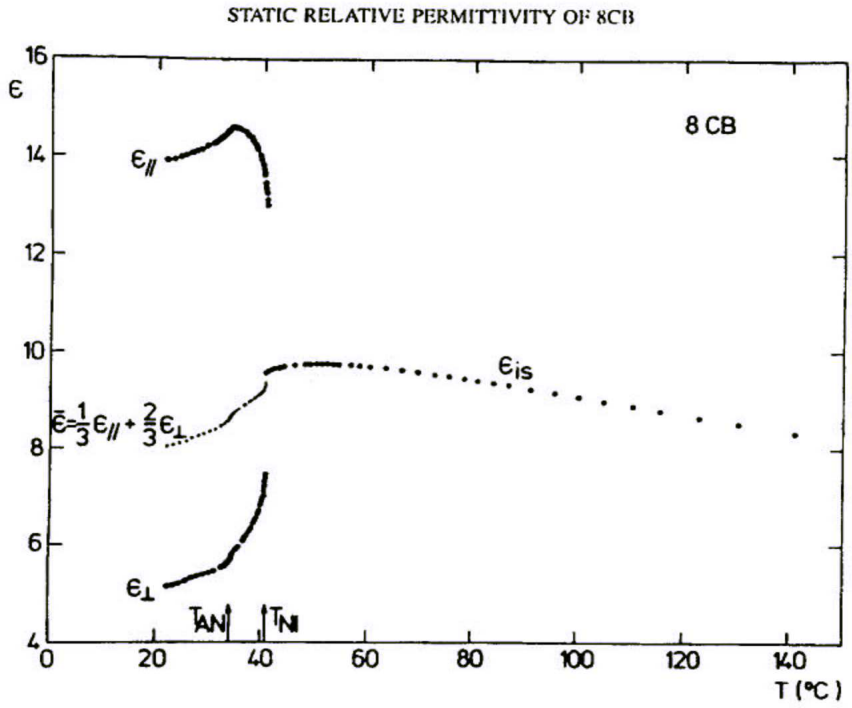

Figure 4.11. The plot was extracted from the work of J. Thoen and G. Menu (see Ref. [50]) and it represents a temperature scan of pure 8CB liquid crystal in the following three cases: magnetic field aligning parallel with measuring electric field, aligning perpendicular, and not under the influence of the magnetic field.

the value of the bulk. The values for $\rho_S = 0.03$ g cm^{-3} were affected by artifacts not showing a clean behavior. Figures 4.14 and 4.15 show the data obtained with the above formula Eq. (4.17). As a general idea all the values are under-unit which is correct. The values for the bulk are the highest which again is understandable by the fact that QRD disturbs the alignment. Moreover the data give the same range of values as had been shown in the paper cited above.

The second test we can relay on is to compare the samples before and after the annealing as phase transition temperatures. Figure 4.16 for the second-order N-SmA transition and Fig. 4.17 for the first-order I-N transition. Both tell the same thing: the transition temperature is increasing. There is an initial increase just after the zero field procedure and again another one after the annealing itself.

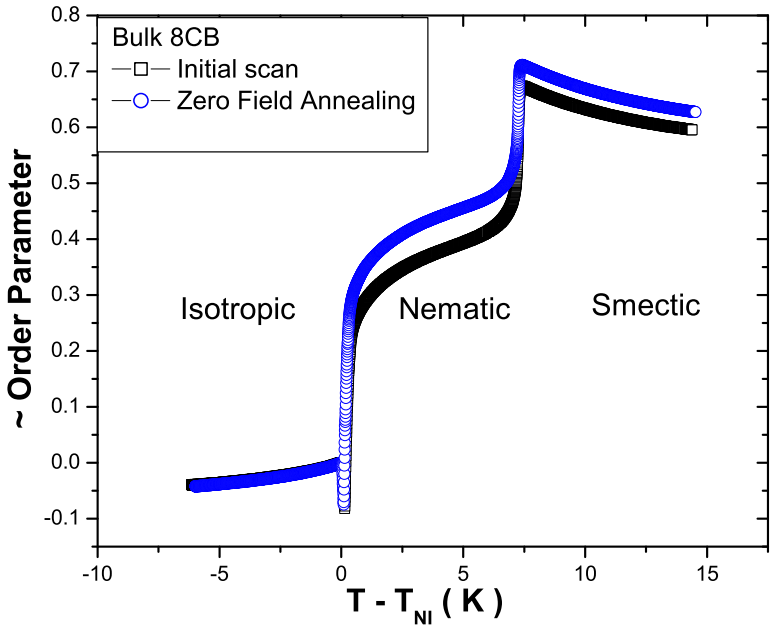

Figure 4.12. The quantity which is proportional to the order parameter for the bulk 8CB before and after a "zero" field annealing procedure preceded and followed by cooling scans.

The shape of the dependency of the transition temperature of density is the same for all three cases.

In the previous two chapters, we indicated that the magnetic field is producing an opposite effect on the transition temperature. For the electric field the two tests give the same conclusion, that the order is decreasing. Thus, magnetic field is increasing the order but the electric field is decreasing it. There is no contradiction in that. The magnetic field applied was constant versus an alternating electric field. Acting continuously, the magnetic field could rearrange the silica colloid by making it more rigid. We speculate that an alternating field is breaking the domains so more domains mean more energy to spend to go to a more disordered phase which leads to an increase in the transition temperature. The same conclusion was drawn by J. Thoen and collaborators [54] speaking for 5CB liquid crystal.

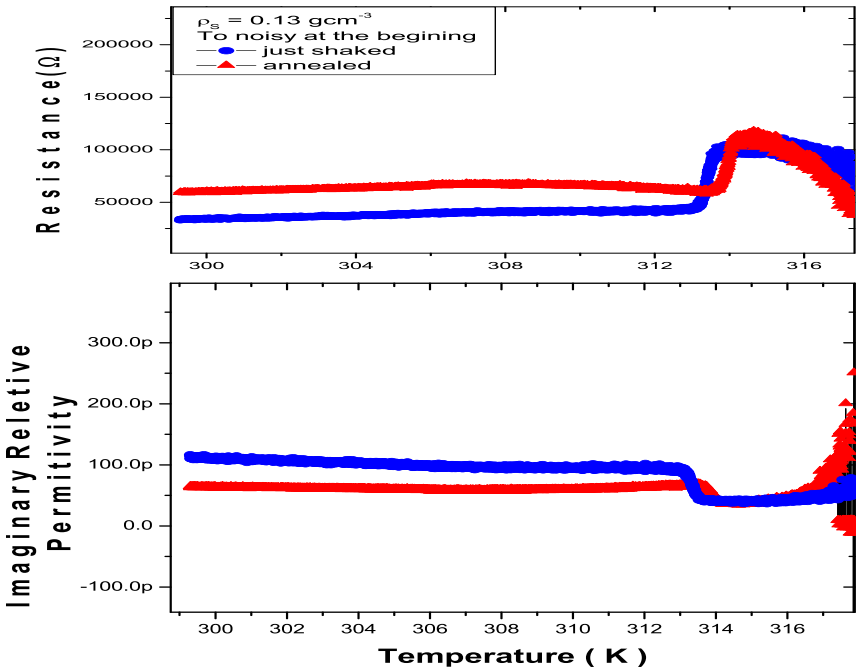

Figure 4.13. Resistance(top) and imaginary relative permittivity for the ρ_S = 0.13 g cm^{-3}, in conjugate density units, 8CB+sil sample.

4.3.3 Liquid Crystal Disorder Hypotheses

This chapter presents an idea regarding liquid crystal in the nematic phase. A paradigm will be tested in explaining the results we obtained along with any results obtained in liquid crystal experiments. The main idea is that liquid crystals molecules having an elongated shape, will prefer rotation circumscribing a cylinder rather than a sphere. Thus, in the nematic phase, molecules rotate preferring a direction which we assimilate with the nematic director. The fixed point of the molecule of the bulk, when rotating, is its center of mass. In Fig. 4.18, there are envisioned two types of molecules. The ones out of the vicinity of the beads, behave exactly like the bulk molecules; they are, however, in a "fractal world" when they have any beads around them. That aspect makes the distance from the edges of the blob longer for molecules that are in the middle of it - if it will be only for that

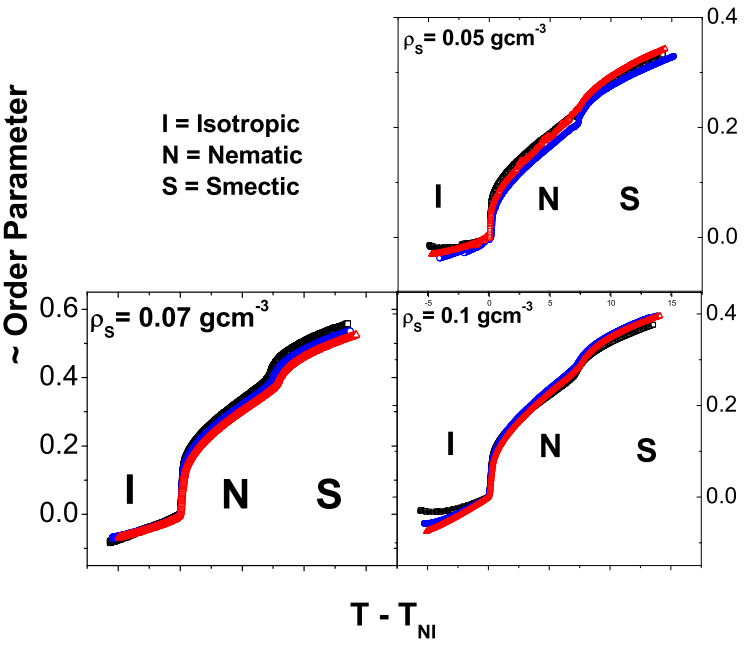

Figure 4.14. The estimated scalar part of the nematic order parameter for 3 different densities of 8CB+sil.

the higher the silica density, the higher the transition temperature would be. Now the molecules that are next to the beads, rotate with a quasi fixed point on the bead. Actually, the molecule and the bead attract each other. Molecules rotate with a precession now with the fixed point at one end. Thus, the molecules around the beads are not in the phase the bulk molecules are in, and they form a layer that thickens the silica strands just limiting the space for the bulk-like molecules. The fact that they are attracted by the beads, causes them to require an energy that is too large to change their state by thermal collisions. Still, one can do that by applying a strong enough external field.

With the described model in mind let us try to explain the phenomena encountered.

The application of an AC electric field make some molecules to snap out of the influence of the beads. The molecules remaining attached to the beads will widen the precession angle, and this way the layer around the bead will be thinner. The

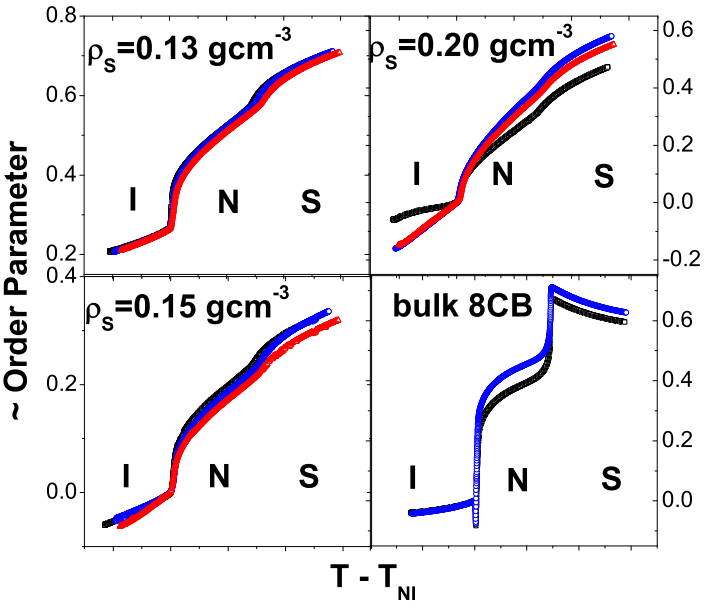

Figure 4.15. The estimated scalar part of the nematic order parameter for the remaining 3 densities of 8CB+sil as well as the bulk resuls.

molecules in the bulk will increase in number. The more molecules in the bulk the bigger the transition temperature.

The magnetic field applying procedure - see first chapter - can be explained in the above paradigm. Everything starts with the cold welding of a cup and lid with the mixture in between the two. That leads the fractal structure of the silica colloids to be distorted in a ring around the edges. Thus, some molecules were pushed in the bulk right from the sample formation. When the molecules are under the influence of a very intense magnetic field, some of them will reconnect with the silica bead and the number of molecules in the bulk diminishes. The less molecules in the bulk the smaller the energy required for the transition so the smaller transition temperature is noticed. The ring where the molecules are affected is big enough to accommodate sufficient molecules and thin enough as well. A brief inspection of the cold welding envelope will tell that size would make a difference in the way discussed previously .

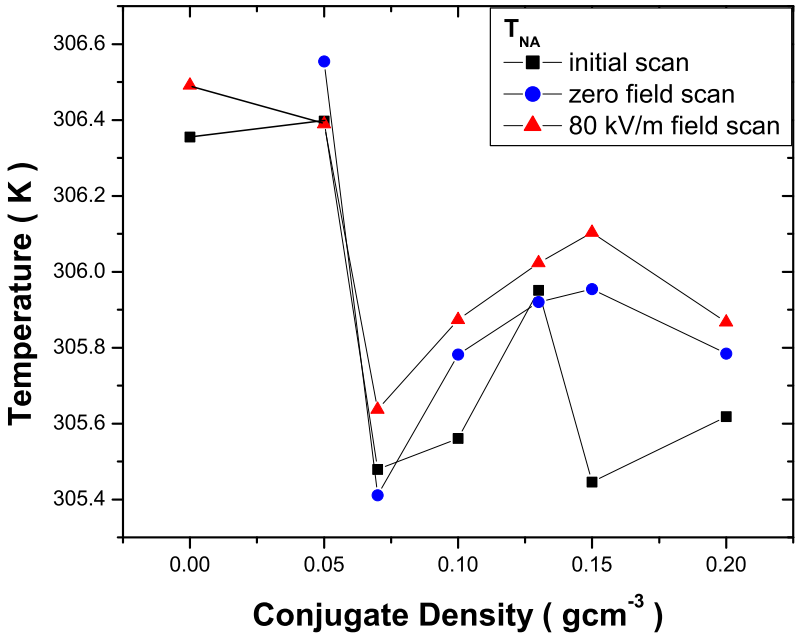

Figure 4.16. The nematic to smectic-A transition temperature for the three stages.

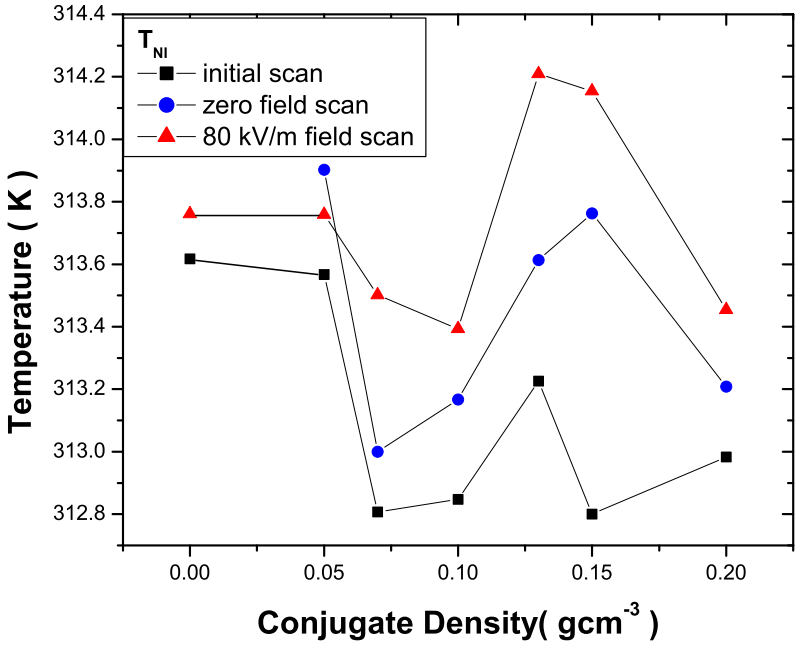

Figure 4.17. The nematic-isotropic temperature transition for the three stages.

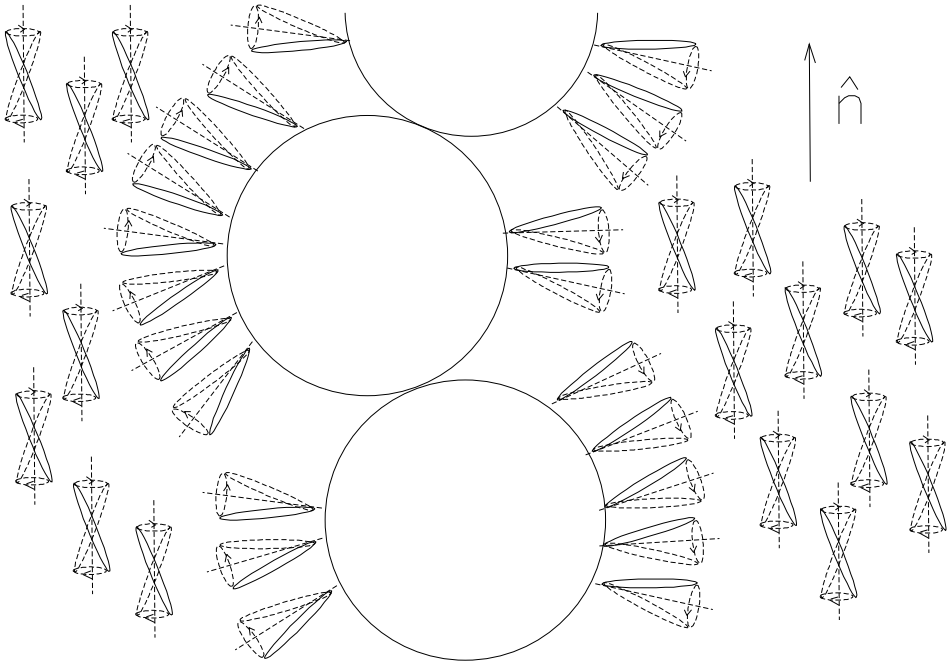

Figure 4.18. The second schematic picture of the rod-like molecules of a generic liquid crystal and silica beads.

Chapter 5

CONCLUSIONS

The two techniques applied to aligned 8CB+sil samples in this thesis have important outcomes. These results are considered relatively robust in that two control samples (of low and high density) experienced identical thermal history but in the absence of any external field. These control samples reproduced well previously reported results of unaligned random 8CB+sil samples.

The results of the application of an external uniform magnetic and ac-electric fields to six densities of an aerosil and 8CB liquid crystal colloidal mixtures are apparent at both the I-N and N-SmA phase transitions. On average, the N-SmA transition temperature is shifted down by $\sim$ 150 mK and by $\sim$ 350 mK for I-N transition with respect to the unaligned random mixture samples. One possible mechanism may be due to the silica aerosil gel structure becoming more rigid (more aerogel-like) as the alignment procedure (repeated thermal cycling in the presence of an external field) alters the initially fractal-like gel into one more foam-like. A more rigid gel would be more disordering. This mechanism is thought to account for a similar shift in transition temperatures for the 8OCB+sil system after crystallization [43]. However, low-angle x-ray studies on identically prepared aligned samples do not indicate any significant changes in the background scattering due to the aerosil gel [48]. Of course, changes in the gel structure could have occurred on much longer length scales, but this would be difficult to reconcile with a presumably increased rigidity.

Furthermore, the nematic range (the difference in temperature between the I-N and N-SmA) becomes smaller and nearly ρ_S independent for the aligned samples.

This reducing in nematic range indicates that orientational order, though uniform, is *less* stable after alignment relative to the smectic order.

The critical exponent α appears to stabilize to the 3D-XY value of -0.013 for all the densities in hand. The behavior for the unaligned samples was a decreasing trend with respect to the increase of silica density. The values of α were verified with the ones given by the x-ray scattering of Leheny et. al. [48] 3.3.

We also speculate that, due to the alignment, the silica lattice was rearranged in a way that the average mean void became a little bigger and also the silica structure became more rigid. Therefore, by the combined action of the liquid crystal molecules, a new equilibrium relative position has been achieved. This position could not been achieved when the gel was formed. In that process, the lattice formed just with local influence by the time the acetone was leaving the site. Now, during the alignment, liquid crystal molecules are "pushing", due to their magnetic dipole, in one direction only (It was an unidirectional magnetic field.). Also, because the temperature was ramped up and down around the nematic-isotropic transition temperature, the newly formed nematic domains, while cooling, will have a preferred order parameter direction for all of them. This last fact makes the strength of the influence of the liquid crystal molecules against the silica lattice even stronger.

The data we got for the I-N coexistence region size shows that the nematic director had not changed its elasticity in the process of alignment. For the part of the enthalpy that we had found smaller after the density of 0.07 g cm^{-3} we do not have enough data to draw a conclusion. A nonadiabatic calorimetric study of the aligned samples would useful and shed further light on the two-step transition process.

Finally, the side by side aligned and random densities are being presented in Figs. 2.2 and 2.3. For the 0.05 g cm^{-3} density, one can see very clearly that the aligned sample has a bigger enthalpy in both of the two processes than was encountered during the first order transition. The imaginary enthalpy graph shows the opposite of the real one. This can be explained by the fact that the amount of order which makes the heat loss sideways (not reaching the thermometer) is smaller. One should notice the difference in magnitude between the two enthalpies. As for the 0.13 g cm^{-3}, it is a similar explanation with the particularity that the

second kind of process is dominant now.

In the dielectric experiment, the transition temperatures increased as a result of the application of a strong alternating electric field. The intensity of the field was chosen to represent the same range of forces that the magnetic field would produce in the first experiment. Another effect of the alignment was that the capacitance went higher after applying successive higher and higher pulses of alternating electric field.

Here the explanations are could be due to a different cause. Firstly, the electric field applied was alternating. Rather than increasing the rigidity the silica lattice, the electric field could change the distribution of molecules in the layer surrounding the silica beads. That could be either a rearrange more closer to a parallel to the electric field position or, yanking some of the molecules from the mentioned layer or both.

For the future one can continue the especially the dielectric experiment. A more rigourously procedure in terms of avoiding any impurity (including water) should be pursued. Also can be used higher intensity electric field. A complementary experiment with the constituents would be a dilatometry one. A DNMR (deuterium nuclear magnetic resonance) with the hydrogen bonds at silica beads partially replaced by deuterium will reveal the change in silica lattice.

Bibliography

[1] N. Clark, T. Bellini, R. Malzbender, B. Thomas, A. Pappaport, C. Muzny, D. Shaefer, and L. Hrebesh, *Phys. Rev. Lett.* **71**, 3505 (1993).

[2] T. Bellini, N. Clark, and D. Shaefer, *Phys. Rev. Lett.* **74**, 2740 (1995).

[3] H. Zeng, B. Zalar, G. Iannacchione and, D. Finotello, *Phys. Rev.* E **60**, 5607 (1999).

[4] G. S. Iannacchione, D. Finotello, L. V. Natarajan, R. L. Sutherland, V. P. Tondiglia, T. J. Bunning, and W. W. Adams, "Deuterium NMR and morphology study of polymer-dispersed liquid-crystal Bragg gratings", *Europhys. Lett.* **36**(6), 425-430 (1996).

[5] G. S. Iannacchione and D. Finotello, "Specific heat dependence on orientational order at cylindrically confined liquid crystal phase transitions", *Phys. Rev.* E **50**(6), 4780-95 (1994).

[6] C. W. Garland and G. Nounesis, "Critical behavior at the nematic-smectic-A transition", *Phys. Rev.* E **49**(4), 2004 (1995).

[7] G. S. Iannacchione, C. W. Garland, J. T. Mang, and T. P. Rieker, "Calorimetric and small angle x-ray scattering study of phase transitions in octylcyanobiphenyl-aerosil dispersions", *Phys. Rev.* E **58**(5), 5966-81 (1998).

[8] P. G. de Genes and J. Prost, *The Physics of Liquid Crystals* (Oxford Science Publications, Oxford, England, 1993).

[9] L. D. Landau and E. D. Lifshitz, *Statistical Physics* (Reed Education and Professional Publishing Ltd., Oxford, England, 2000).

[10] , P. F. Sullivan and G. Seidel, "Title", *Phys. Rev.* **173**, 679 (1968).

[11] L. Radzihovsky and J. Toner, "Nematic to smectic-A transition in aerogel", *Phys. Rev. Lett.* **79**(21), 4214-17 (1997).

[12] L. Radzihovsky and J. Toner, "Smectic liquid crystals in random environments", *Phys. Rev.* B **60**(1), 206 (1999).

[13] B. Jacobsen, K. Saunders, L. Radzihovsky, and J. Toner, "Two new topologically ordered glass phases of smectics confined in anisotropic random media", *Phys. Rev. Lett.* **83**(7), 1363-66 (1999).

[14] K. Saunders, B. Jacobsen, L. Radzihovsky, J. Toner, "Topologically ordered phases of smectics confined in anisotropic random media: smectic Bragg glasses", *J. Phys.: Condens. Matt.* **12**, A215 (2000).

[15] F. Mercuri, U. Zammit, and M. Marinelli, "Effect of the nematic range on the critical behavior and anisotropy of the heat transport parameters at the smectic-Anematic phase transition", *Phys. Rev.* E **57**(1), 596 (1998).

[16] D. Liang, M. A. Borthwick, and R. L. Leheny, "Smectic liquid crystals in anisotropic colloidal silica gels", *J. Phys.: Condens. Matt.* **16**(19), S1989 (2004).

[17] Y. Imry and S.-K. Ma, "Random-field instability of the ordered state of continuous symmetry", *Phys. Rev. Lett.* **35**(21), 1399-1401 (1975).

[18] D. E. Feldman, "Quasi-long-range order in the random anisotropy Heisenberg model: Functional renormalization group in $4-\epsilon o$ dimensions", *Phys. Rev.* B **61**(1), 382-390 (2000).

[19] G. S. Iannacchione, S. Park, C. W. Garland, R. J. Birgeneau, and R. L. Leheny, "Smectic ordering in liquid-crystal-aerosil dispersions. II. Scaling analysis", *Phys. Rev.* E **67**(1), 11709 (2003).

[20] Y. Imry and M. Wortis, "Influence of quenched impurities on first-order phase transitions", *Phys. Rev.* B **19**(7), 3580-85 (1979).

[21] T. Bellini, N. A. Clark, V. Degiorgio, F. Mantegazza, and G. Natale, "Light-scattering measurement of the nematic correlation length in a liquid crystal with quenched disorder", *Phys. Rev.* E **57**(3), 2996-3006 (1998).

[22] T. Bellini, M. Buscaglia, C. Chiccoli, F. Mantegazza, P.Pasini, and C. Zannoni, "Nematics with quenched disorder: What is left when long range order is disrupted?", *Phys. Rev. Lett.* **85**(5), 1008-1011 (2000).

[23] T. Bellini, M. Buscaglia, C. Chiccoli, F. Mantegazza, P. Pasini, and C. Zannoni, "Nematics with quenched disorder: How long will it take to heal?", *Phys. Rev. Lett.* **88**(24), 245506 (2002).

[24] M. Marinelli, A. K. Ghosh, and F. Mercuri, "Small quartz silica spheres induced disorder in octylcyanobiphenyl (8CB) liquid crystals: A thermal study", *Phys. Rev.* E **63**(6), 061713 (2001).

[25] S. Park, R. L. Leheny, R. J. Birgeneau, J.-L. Gallani, C. W. Garland, and G. S. Iannacchione, "Hydrogen-bonded silica gels dispersed in a smectic liquid crystal: A random field XY system", *Phys. Rev.* E **65**(5), 50703 (2002).

[26] R. L. Leheny, S. Park, R. J. Birgeneau, J.-L. Gallani, C. W. Garland, and G. S. Iannacchione, "Smectic ordering in liquid-crystal-aerosil dispersions I. X-ray scattering", *Phys. Rev.* E **67**(1), 11708 (2003).

[27] C. C. Retsch, I. McNulty, and G. S. Iannacchione, "Elastic coupling of silica gel dynamics in a liquid-crystal in aerosil dispersion", *Phys. Rev.* E **65**(3), 32701 (2002).

[28] T. Jin and D. Finotello, "Aerosil dispersed in a liquid crystal: Magnetic order and random silica disorder", *Phys. Rev. Lett.* **86**(5), 818-21 (2001).

[29] M. Caggioni, A. Roshi, S. Barjami, F. Montegazza, G. S. Iannacchione, and T. Bellini, "Isotropic to nematic transition of aerosil-disordered liquid crystals", *Phys. Rev. Lett.* **93**, 127801 (2004).

[30] A. Guinier, *X-ray diffraction in crystals, imperfect crystals, and amorphous bodies* (1st edition, W. H. Freeman Press, San Francisco, 1963).

[31] W. H. Press, *Numerical Recipes in C* (2nd edition, Cambridge University Press, New York, 1997)

[32] G. Porod, chapter 2, *Small angle x-ray scattering* (1st edition, O. Glatter and O. Kratky editors, Academic Press, 1982).

[33] H. Yao, K. Ema, and C. W. Garland, "Nonadiabatic scanning calorimeter", *Rev. Sci. Instrum.* **69**, 172 (1998).

[34] M. J. P. Gingras, "Ordering of liquid-crystals in porous media", private communication (1998).

[35] M. Marinelli, F. Mercuri, U. Zammit, and F. Schudieri, "Dynamic critical behavior of thermal parameters at the smectic-Anematic phase transition of octyloxythiolbenzoate", *Phys. Rev.* E **53**(1), 701-05 (1996).

[36] B. Zhou, G. S. Iannacchione, C. W. Garland, and T. Bellini, "Random-field effects on the nematic - smectic-A phase transition due to silica aerosil particles", *Phys. Rev.* E **55**(3), 2962 (1997).

[37] T. Bellini, L. Radzihovsky, J. Toner, and N. A. Clark, "Universality and scaling in the disordering of a smectic liquid crystal", *Science* **294**, 1074 (2001).

[38] P. Jamee, G. Pitsi, and J. Thoen, "Systematic calorimetric investigation of the effect of silica aerosils on the nematic to isotropic transition in heptylcyanobiphenyl", *Phys. Rev.* E **66**(2), 021707-8 (2002).

[39] P. S. Clegg, C. Stock, R. J. Birgeneau, C. W. Garland, A. Roshi, and G. S. Iannacchione, "Effect of a quenched random field at a continuous symmetry breaking transition: nematic to smectic-A in an octyloxycyanobiphenyl-aerosil dispersion", *Phys. Rev.* E **67**, 021703 (2003).

[40] Z. Kutnjak, S. Kralj, G. Lahajnar, and S. Žumer, "Calorimetric study of octylcyanobiphenyl liquid crystal confined to a controlled-pore glass", *Phys. Rev.* E **68**(2), 021705 (2003).

[41] R. Bandyopadhyay, D. Liang, R. H. Colby, J. L. Harden, and R. L. Leheny, "Enhanced elasticity and soft glassy rheology of a smectic in a random porous environment", *Phys. Rev. Lett.* **94**(10), 107801 (2005).

[42] T. Jin and D. Finotello, "Controlling disorder in liquid crystal aerosil dispersions", *Phys. Rev.* E **69**(4), 041704 (2004).

[43] A. Roshi, G. S. Iannacchione, P. S. Clegg, and R. J. Birgeneau, "Evolution of the isotropic-to-nematic phase transition in octyloxycyanobiphenyl+aerosil dispersions", *Phys. Rev.* E **69**(3), 031703-14 (2004).

[44] A. Roshi, G. S. Iannacchione, P. S. Clegg, R. J. Birgeneau, and M. E. Neubert, "Calorimetric study of the nematic to smectic-A and smectic-A to smectic-C phase transitions in liquid-crystal – aerosil dispersions", *Phys. Rev.* E **72**(5), 051716 (2005).

[45] A. Roshi, S. Barjami, D. Paterson, I. McNulty, and G. S. Iannacchione, "Structure and dynamics of a nano-colloidal silica gel dispersion", *Phys. Rev.* E **74**(3), 031404-8 (2006).

[46] L. Wu, B. Zhou, C. W. Garland, T Bellini, and D. W. Schaefer, "Heat-capacity study of nematic-isotropic and nematic-smectic-A transitions for octylcyanobiphenyl (8CB) in silica aerogels", *Phys. Rev.* E **51**(3), 2157 (1995).

[47] H. Yao, T. Chan, and C. W. Garland, "Smectic-Csmectic-I critical point in a liquid crystal mixture: Static and dynamic thermal behavior", *Phys. Rev.* E **51**, 4585-97 (1995).

[48] D. Liang and R. L. Leheny, "Smectic liquid crystals in anisotropic random enviroment", *Phys. Rev.* E **75**(3), 031705 (2007).

[49] D. Sharma and G. S. Iannacchione, "Role of an aerosil dispersion on the activated kinetics of an LC1-xSilx system", *J. Phys. Chem.* **B110**(51), 26160-9 (2006).

[50] J. Thoen and G. Menu, "Temperature dependence of the static relative permitivity of octylcyanubiphenil 8CB", *Mol. Cryst. Liq. Cryst.* **97**, 163-176 (1983).

[51] T. K. Bose, B. Champbell, S. Yagihara, and J. Thoen, "Dielectric-relaxation study of alkylcyanobiphenyl liquid crystals using time-domain spectroscopy", *Phys. Rev.* A **36**(12), 5767 (1987).

[52] A. Hourri, T. K. Bose, and J. Thoen, "Effect of silica dispersions on the dielectric properties of a nematic liquid crystal", *Phys. Rev.* E **63**(5), 051702 (2001).

[53] J. Leys, G. Sinha, C. Glorieux, and J. Thoen, "Influence of nanosized confinements on 4-n-decyl-4-cyanobiphenyl (10CB): A broadband dielectric study", *Phys. Rev.* E **71**(5), 051709 (2005).

[54] G. Sinha, J. Leys, C. Glorieux, and J. Thoen, "Dielectric spectroscopy of aerosil-dispersed liquid crystal embedded in anopore membranes", *Phys. Rev.* E **72**(5), 051710 (2005).

[55] G. P. Sinha and F. M. Aliev, "Dielectric spectroscopy of liquid crystals in smectic, nemetic and isotropic phases confined in random porous media", *Phy. Rev.* E **58**(2), 2001 (1998).

[56] F. M. Aliev, Z. Nazario, and G. P. Sinha, "Broadband dielectric spectroscopy of confined liquid crystals, *J. Non-Cryst. Solids* **305**(1-3), 218-225 (2002).

[57] M. R. Bengoechea and F. M. Aliev, "Dielectric relaxation in thin liquid crystal leyers formed on cylindrical pores walls", *J. Non-Cryst. Solids* **351**(33-36), 2685-89 (2005).

[58] F. M. Aliev, M. R. Bengoechea, C. Y. Gao, H. D. Cochran, and S. Dai, "Dielectric relaxation in liquid crystals confined in a quasi-one-dimensional system", *J. Non-Cryst. Solids* **351**(33-36), 2690-93, (2005).